

# 1 **Missing Peroxy Radical Sources within a Summertime**

## 2 **Ponderosa Pine Forest**

3 **G. M. Wolfe<sup>1,a,b</sup>, C. Cantrell<sup>2,c</sup>, S. Kim<sup>2,d</sup>, R. L. Mauldin III<sup>2,3,c</sup>, T. Karl<sup>2,e</sup>, P. Harley<sup>2</sup>,**  
4 **A. Turnipseed<sup>2</sup>, W. Zheng<sup>2</sup>, F. Flocke<sup>2</sup>, E. C. Apel<sup>2</sup>, R. S. Hornbrook<sup>2</sup>, S. R. Hall<sup>2</sup>, K.**  
5 **Ullmann<sup>2</sup>, S. B. Henry<sup>1</sup>, J. P. DiGangi<sup>1,f</sup>, E. S. Boyle<sup>1</sup>, L. Kaser<sup>4,g</sup>, R. Schnitzhofer<sup>4</sup>,**  
6 **A. Hansel<sup>4</sup>, M. Graus<sup>5</sup>, Y. Nakashima<sup>6, h</sup>, Y. Kajii<sup>7</sup>, A. Guenther<sup>2,i</sup>, and F. N. Keutsch<sup>1</sup>**

7 [1]{Department of Chemistry, University of Wisconsin, Madison, WI, USA}

8 [2]{Atmospheric Chemistry Division, National Center for Atmospheric Research, Boulder, CO,  
9 USA}

10 [3]{Department of Physics, University of Helsinki, Helsinki, Finland}

11 [4]{Institute of Ion Physics and Applied Physics, University of Innsbruck, Innsbruck, Austria}

12 [5]{Chemical Sciences Division, NOAA Earth System Research Laboratory, Boulder, CO,  
13 USA}

14 [6]{Division of Applied Chemistry, Faculty of Urban Environmental Sciences, Tokyo  
15 Metropolitan University, Tokyo, Japan}

16 [7]{Graduate School of Global Environmental Studies, Kyoto University, Kyoto, Japan}

17 [a]{Now at Joint Center for Earth Systems Technology, University of Maryland Baltimore  
18 County, Baltimore, MD, USA}

19 [b]{Now at Atmospheric Chemistry and Dynamics Laboratory, NASA Goddard Space Flight  
20 Center, Greenbelt, MD, USA}

21 [c]{Now at Department of Atmospheric and Oceanic Sciences, University of Colorado, Boulder,  
22 CO, USA}

23 [d]{Now at Department of Earth System Science, University of California, Irvine, CA, USA}

24 [e]{Now at Institute for Meteorology and Geophysics, University of Innsbruck, Innsbruck,  
25 Austria}

1 [f]{Now at Department of Civil & Environmental Engineering, Princeton University, Princeton,  
2 NJ, USA }

3 [g]{Now at Atmospheric Chemistry Division, National Center for Atmospheric Research,  
4 Boulder, CO, USA }

5 [h]{Now at Department of Environmental and Natural Resource Science, Faculty of Agriculture,  
6 Tokyo University of Agriculture and Technology, Tokyo, Japan }

7 [i]{Now at Atmospheric Sciences and Global Change Division, Pacific Northwest National  
8 Laboratory, Richland, WA USA }

9

## 10 **Abstract**

11 Organic peroxy ( $\text{RO}_2$ ) and hydroperoxy ( $\text{HO}_2$ ) radicals are key intermediates in the  
12 photochemical processes that generate ozone, secondary organic aerosol and reactive nitrogen  
13 reservoirs throughout the troposphere. In regions with ample biogenic hydrocarbons, the richness  
14 and complexity of peroxy radical chemistry presents a significant challenge to current-generation  
15 models, especially given the scarcity of measurements in such environments. We present peroxy  
16 radical observations acquired within a Ponderosa pine forest during the summer 2010 Bio-hydro-  
17 atmosphere interactions of Energy, Aerosols, Carbon,  $\text{H}_2\text{O}$ , Organics and Nitrogen – Rocky  
18 Mountain Organic Carbon Study (BEACHON-ROCS). Total peroxy radical mixing ratios reach  
19 as high as 180 pptv and are among the highest yet recorded. Using the comprehensive  
20 measurement suite to constrain a near-explicit 0-D box model, we investigate the sources, sinks  
21 and distribution of peroxy radicals below the forest canopy. The base chemical mechanism  
22 underestimates total peroxy radicals by as much as a factor of 3. Since primary reaction partners  
23 for peroxy radicals are either measured ( $\text{NO}$ ) or under-predicted ( $\text{HO}_2$  and  $\text{RO}_2$ , i.e. self-  
24 reaction), missing sources are the most likely explanation for this result. A close comparison of  
25 model output with observations reveals at least two distinct source signatures. The first missing  
26 source, characterized by a sharp midday maximum and a strong dependence on solar radiation, is  
27 consistent with photolytic production of  $\text{HO}_2$ . The diel profile of the second missing source  
28 peaks in the afternoon and suggests a process that generates  $\text{RO}_2$  independently of sun-driven  
29 photochemistry, such as ozonolysis of reactive hydrocarbons. The maximum magnitudes of these

1 missing sources ( $\sim 120$  and  $50$  pptv  $\text{min}^{-1}$ , respectively) are consistent with previous observations  
2 alluding to unexpectedly intense oxidation within forests. We conclude that a similar mechanism  
3 may underlie many such observations.

4

## 5 **1 Introduction**

6 Peroxy radicals are central components of the tropospheric radical pool. Organic peroxy radicals  
7 ( $\text{RO}_2$ ) are metastable intermediates in the oxidation of volatile organic compounds (VOC) (R1),  
8 while hydroperoxyl radicals ( $\text{HO}_2$ ) are generated via photolysis of carbonyl-containing VOC  
9 (e.g. formaldehyde) (R2), alkene ozonolysis (R3) and radical cycling reactions (R5, R6).  $\text{RO}_2$   
10 and  $\text{HO}_2$  typically exhibit lifetimes of 1 to 1000 s with respect to reaction with nitric oxide (NO)  
11 (R4, R5) and other peroxy radicals (R7, R8, R9); larger  $\text{RO}_2$  may also undergo isomerization  
12 and/or unimolecular decomposition. Together with the hydroxyl (OH) and alkoxy (RO) radicals,  
13 these species comprise the  $\text{RO}_x$  radical family. Rapid cycling among  $\text{RO}_x$  and the nitrogen oxide  
14 radicals ( $\text{NO}_x = \text{NO} + \text{NO}_2$ ) lies at the core of photochemical mechanisms that regulate  
15 atmospheric composition and its associated impacts on air quality and climate.



25 A number of key processes hinge upon the fate of peroxy radicals. For example, the  
26 conversion of NO to  $\text{NO}_2$  via (R4) and (R5) is a critical step in tropospheric ozone formation  
27 (Thornton et al., 2002). Reactions of  $\text{RO}_2$  with NO and  $\text{NO}_2$  may also form alkyl nitrates and

1 peroxy nitrates, respectively, facilitating the redistribution of pollutant precursors over regional  
2 and global scales (Moxim et al., 1996;Paulot et al., 2012;Browne and Cohen, 2012). Conversely,  
3 cross-reactions of peroxy radicals ((R7) - (R9)) are responsible for termination of radical cycling  
4 in high-VOC, low-NO<sub>x</sub> regimes. These reactions also form hydrogen peroxide (H<sub>2</sub>O<sub>2</sub>) and  
5 organic hydroperoxides (ROOH), which can induce oxidative stress in vegetation (Hewitt et al.,  
6 1990). Transformations of RO<sub>2</sub> also generate oxidized VOC that may contribute to formation and  
7 growth of secondary organic aerosol (SOA), a major fraction of the global aerosol burden  
8 (Hallquist et al., 2009). SOA precursor production depends strongly on the degree of  
9 functionalization versus fragmentation (Chacon-Madrid and Donahue, 2011), which in turn  
10 varies with the specific molecular structure of each RO<sub>2</sub> radical. Peroxy radicals themselves can  
11 act as a major source of oxidants via (R4). Because this reaction shifts RO<sub>x</sub> into its more reactive  
12 form while generating NO<sub>2</sub> (a precursor for ozone and thus OH), it effectively amplifies  
13 atmospheric oxidizing capacity. In many environments, this reaction is the main daytime source  
14 of OH (Stone et al., 2012).

15 The structure and abundance of VOC precursors shapes the detailed chemistry of peroxy  
16 radicals. In the remote troposphere, methane and CO are the primary reactants. Here, methyl  
17 peroxy radical (CH<sub>3</sub>O<sub>2</sub>) is the major RO<sub>2</sub> species and HO<sub>2</sub> concentrations typically exceed RO<sub>2</sub>  
18 (Cantrell et al., 2003). Near VOC sources, on the other hand, the RO<sub>2</sub> distribution can be  
19 considerably more complex and the prevailing chemistry is less well understood. This is  
20 particularly true in regions dominated by biogenic alkenes such as isoprene, 2-methyl-3-butene-  
21 2-ol (MBO) and monoterpenes. Numerous field studies have identified gaps in our understanding  
22 of photochemistry in these environments (Carslaw et al., 2001;Faloona et al., 2001;Tan et al.,  
23 2001;Thornton et al., 2002;Lelieveld et al., 2008;Ren et al., 2008;Hofzumahaus et al.,  
24 2009;DiGangi et al., 2011;Whalley et al., 2011;Griffith et al., 2013;Mao et al., 2012;Kim et al.,  
25 2013;Hens et al., 2013), while theoretical and laboratory work continues to reveal new reaction  
26 pathways that can significantly impact oxidant levels and reaction product distributions (Dillon  
27 and Crowley, 2008;Peeters et al., 2009;Peeters and Müller, 2010;da Silva et al., 2010;Crouse et  
28 al., 2011;Wolfe et al., 2012;Crouse et al., 2012;Crouse et al., 2013;Liu et al., 2013). Much of  
29 this work has focused on isoprene, which comprises one third of the global biogenic VOC  
30 emission budget (Guenther et al., 2012). Revised isoprene mechanisms can profoundly impact  
31 model predictions of ozone, aerosol, radicals and reservoir species (Xie et al., 2013;Mao et al.,

1 2013). In most instances, uncertainties in these reaction mechanisms center on the fate of first-  
2 generation  $\text{RO}_2$  and on processes that control the balance of OH,  $\text{HO}_2$  and  $\text{RO}_2$ .

3 Observations of total peroxy radicals in forested environments are relatively sparse.  
4 During the ROSE campaign in rural Alabama, Cantrell et al. (1992;1993) reported typical sunny  
5 mid-day  $\text{RO}_2 + \text{HO}_2$  mixing ratios of 100 to 150 pptv in an isoprene-rich environment under  
6 minimal anthropogenic influence ( $\text{NO} \sim 100$  pptv at noon). Maximum values of up to 300 pptv  
7 were observed on several days, and a steady-state model predicted an  $\text{RO}_2/\text{HO}_2$  ratio of  $\sim 1$  for  
8 one prototypical day. Qi et al. (2005) also observed fairly high  $\text{RO}_2 + \text{HO}_2$  mixing ratios (109 to  
9 134 pptv at midday) above a Japanese mixed deciduous forest with typical  $\text{NO}$  mixing ratios less  
10 than 200 pptv, and it was noted that peroxy radical concentrations consistently peaked  $\sim 3$  hours  
11 after solar noon. At the PROPHET site in Northern Michigan, Mihele and Hastie (2003)  
12 measured midday  $\text{RO}_2 + \text{HO}_2$  ranging from 20 to 60 pptv. As in Qi et al. (2005), peroxy radicals  
13 at PROPHET were found to peak several hours after solar noon, indicating an important role for  
14 processes other than primary radical production. More recently, Griffith et al. (2013) reported  
15 midday mixing ratios of 20 to 50 pptv for the sum of  $\text{HO}_2$  and first-generation isoprene peroxy  
16 radicals at PROPHET during summer of 2008 and 2009, consistent with earlier observations.  
17 Observations of  $\text{HO}_2$  are more ubiquitous and are reviewed elsewhere (Stone et al., 2012),  
18 though some of these measurements may contain positive artifacts due to alkene-derived  $\text{RO}_2$   
19 (Fuchs et al., 2011). Investigations of  $\text{RO}_x$  cycling are often constrained with measurements of  
20 OH and  $\text{HO}_2$  but rarely include a constraint on  $\text{RO}_2$ . Since  $\text{RO}_2$  can comprise half or more of the  
21 total peroxy radical budget, such observations are crucial for identifying and eliminating gaps in  
22 chemical mechanisms.

23 We present an analysis of peroxy radical measurements obtained within a Ponderosa pine  
24 forest during the 2010 Bio-hydro-atmosphere interactions of Energy, Aerosols, Carbon,  $\text{H}_2\text{O}$ ,  
25 Organics and Nitrogen – Rocky Mountain Organic Carbon Study (BEACHON-ROCS). Using  
26 the comprehensive suite of observations to constrain a near-explicit 0-D chemical box model, we  
27 examine the diel cycle of sources, sinks and partitioning of peroxy radicals in this biogenic  
28 environment. Model underestimation of daytime peroxy radical concentrations leads us to  
29 consider potential missing radical sources. We quantify these missing processes and place them  
30 within the context of canonical chemistry. Analyzing the temporal profiles of missing peroxy

1 radical mixing ratios and production rates, we identify potential novel mechanisms of radical  
2 generation that are consistent with previous anomalous observations at this and other forests.

3

## 4 **2 Methods**

### 5 **2.1 Field Campaign**

6 BEACHON-ROCS took place from 1 – 31 August 2010 at the Manitou Forest Observatory  
7 (39°06'00"N, 105°05'30"W, 2286 m above sea level) Site characteristics and project details are  
8 presented elsewhere (Ortega et al., 2014). The research site is situated within a Ponderosa pine  
9 forest with an average canopy height of 18.5 m and no significant understory. A leaf area index  
10 (LAI) of 3 for the tree canopy and a tree cover fraction of 0.38 gives a landscape average LAI of  
11 1.14. The closest major urban areas are Colorado Springs (33 km SE) and Denver (70 km N).  
12 The site is occasionally impacted by anthropogenic air masses, but prevailing winds bring  
13 relatively clean air from the south and southwest. We have not screened the data for  
14 anthropogenic influence, but visual inspection reveals no obvious dependence of peroxy radical  
15 mixing ratios on wind direction. Major biogenic VOC emissions at this site include 2-methyl-3-  
16 butene-2-ol (MBO), monoterpenes (MT) and methanol (Kaser et al., 2013a;Kaser et al., 2013b).  
17 Isoprene mixing ratios are typically less than 300 pptv, as this compound is only emitted from  
18 Ponderosa pine at very low rates (Kaser et al., 2013a). Further details on the site and  
19 observations can be found elsewhere (DiGangi et al., 2011;DiGangi et al., 2012;Karl et al.,  
20 2012;Kim et al., 2013;Kaser et al., 2013a;Kaser et al., 2013b).

21

### 22 **2.2 Peroxy Radical Measurements**

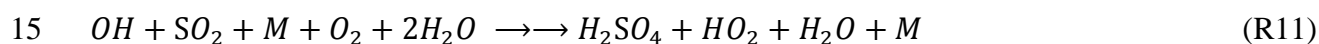
23 Two classes of peroxy radicals were measured via Peroxy Radical Chemical Ionization Mass  
24 Spectrometry (PeRCIMS), described in detail previously (Edwards et al., 2003;Hornbrook et al.,  
25 2011). The instrument was housed in a trailer on the forest floor with the inlet protruding 0.5 m  
26 from the trailer wall at a height of 1.6 m and oriented to the southeast. The upper part of the  
27 PeRCIMS inlet is isolated from sunlight by shielding it with black felt cloth inside the inlet  
28 pylon, thereby minimizing the impact of potential artifacts from solar radiation to negligible

1 levels. The inlet is maintained at a minimum temperature of 10 °C; for the conditions of  
2 BEACHON-ROCS, the heater rarely was active. The typical sample residence time is 0.18 s in  
3 the chemical reaction region and 0.4 s in the ion reaction region. A picture of the trailer and inlet  
4 is included in the supplementary material (Fig. S9).

5 The principle of detection involves three steps. First, ambient air is diluted with either N<sub>2</sub>  
6 or O<sub>2</sub>, followed by addition of varying concentrations of NO and SO<sub>2</sub>. Reaction of HO<sub>2</sub> with NO  
7 generates OH via (R4), while reaction of RO<sub>2</sub> with NO generates an RO radical that can react  
8 either with O<sub>2</sub> to form HO<sub>2</sub> via (R6) or with NO to make RONO.



10 Modulation of the NO/O<sub>2</sub> ratio controls the relative rates of (R6) and (R10) allowing the  
11 PeRCIMS to operate in either an HO<sub>2</sub> (high NO/O<sub>2</sub>) or an RO<sub>2</sub> + HO<sub>2</sub> (low NO/O<sub>2</sub>) measurement  
12 mode. The instrument switches between these two modes every 30 seconds. In the second and  
13 third steps, OH radicals react with SO<sub>2</sub> to generate sulfuric acid, which is then ionized via  
14 reaction with nitrate ions. Ions are detected via a custom-built quadrupole mass spectrometer.



17 Background H<sub>2</sub>SO<sub>4</sub> signals are determined by redirecting the SO<sub>2</sub> flow to the rear of the neutral  
18 reaction region, forcing OH radicals generated via (R4) to react with the excess NO and form  
19 HONO. Generally, the duration of ambient and background measurements is equal. Peroxy  
20 radical mixing ratios are reported as 1-minute averages, with an uncertainty of ±35% and a  
21 detection limit of 2 pptv (for signal/noise = 2) for data from each measurement mode.

22 HO<sub>2</sub> measurements acquired via titration with NO can contain positive artifacts due to  
23 partial conversion of RO<sub>2</sub>, especially when the RO<sub>2</sub> radicals are produced via OH addition to  
24 alkenes. The primary type of RO<sub>2</sub> interfering in the HO<sub>2</sub> measurement are likely β-  
25 hydroxyalkylperoxy radicals (βRO<sub>2</sub>), formed via OH addition to alkenes (Fuchs et al.,  
26 2011;Hornbrook et al., 2011;Whalley et al., 2013a). Upon reaction with NO in the PeRCIMS  
27 inlet, these radicals quickly decompose to make an HO<sub>2</sub> radical that is then detected with nearly  
28 the same efficiency as ambient HO<sub>2</sub>. Laboratory experiments have shown that, relative to  
29 ambient HO<sub>2</sub>, the PeRCIMS sensitivity to isoprene-derived RO<sub>2</sub> is ~12% higher, while that to

1 aromatic RO<sub>2</sub> is ~12% lower (Hornbrook et al., 2011). Sensitivities to other β-  
2 hydroxyalkylperoxy radicals have not been tested, but we assume their chemistry will be similar.  
3 For this reason, we define two quantities:

$$4 \text{ HO}_2^* = \text{HO}_2 + \beta\text{RO}_2 \quad (1)$$

$$5 \text{ RO}_2^* = \text{HO}_2 + \text{RO}_2 - \text{HO}_2^* \quad (2)$$

6 HO<sub>2</sub>\* represents the “HO<sub>2</sub> mode” observations, which we assume to include HO<sub>2</sub> and βRO<sub>2</sub>.  
7 RO<sub>2</sub>\* denotes the difference between total peroxy radicals and HO<sub>2</sub>\*, representing an  
8 operationally-defined subset of the RO<sub>2</sub> pool. The partitioning of total RO<sub>2</sub> between HO<sub>2</sub>\* and  
9 RO<sub>2</sub>\* is discussed further in Section 2.4 and Section 4.

10

### 11 **2.3 Other Measurements**

12 Additional observations used in this analysis include OH, NO, NO<sub>2</sub>, O<sub>3</sub>, CO, PAN (peroxyacetyl  
13 nitrate), PPN (peroxypropionyl nitrate), formaldehyde, glyoxal, a suite of VOC (MBO, isoprene,  
14 α-pinene, β-pinene, limonene, camphene, a group of non-specified monoterpenes, acetone,  
15 methanol, benzene, toluene, methyl vinyl ketone, methacrolein, acetaldehyde, propanal, n-  
16 butanal, 1,3-butadiene), total OH reactivity, temperature, pressure, relative humidity and NO<sub>2</sub>  
17 photolysis frequencies. Table S1 in the Supplementary Information (SI) summarizes the  
18 measurement techniques and their associated uncertainties. It should be noted that some  
19 measurements were taken at various heights, and the heterogeneity of the forest canopy can lead  
20 to strong vertical concentration gradients for some reactive species (Wolfe et al., 2011a).  
21 Furthermore, the openness of the MFO canopy can also lead to horizontal gradients in  
22 chemistry and composition. Most observations utilized here were taken at a height of 1.6 – 4 m,  
23 within the trunk space of the canopy. These heights are also listed in Table S1. Multi-height  
24 measurements of VOC and NO<sub>x</sub> suggest average vertical concentration gradients of less than 4%  
25 per meter in this region (data not shown). NO<sub>2</sub> photolysis frequencies were measured both above  
26 the canopy and at 2 m (on top of the instrument trailer, just above the OH inlet). We caution that  
27 horizontally-averaged in-canopy radiation is likely higher than represented by this measurement,  
28 as the canopy is relatively open and the J(NO<sub>2</sub>) sensor was co-located with the relatively shaded  
29 OH inlet. Moreover, due to the spatial separation of ~4m between the OH and PeRCIMS inlets,



1 this measurement may not reflect the local conditions at the PeRCIMS inlet. Other photolysis  
2 frequencies, notably  $J(\text{O}_3)$ , are estimated by scaling measured  $J(\text{NO}_2)$  with clear-sky photolysis  
3 frequencies calculated from the Master Chemical Mechanism (MCM) v3.2 parameterization  
4 (Jenkin et al., 1997;Saunders et al., 2003).

5 VOC observations were acquired by four separate instruments, each with particular  
6 measurement heights, time resolution and speciation. A detailed comparison of these  
7 measurements is presented elsewhere (Kaser et al., 2013b). Due to better temporal coverage,  
8 MBO, benzene, toluene and acetaldehyde observations are taken from the University of  
9 Innsbruck PTR-TOF-MS measurements at 25 m. Remaining VOC listed above are taken from  
10 the NCAR trace organic gas analyzer (TOGA) measurements (also at 25 m). Furthermore,  
11 mixing ratios of MBO and monoterpenes, which are emitted by Ponderosa pine, are corrected for  
12 in-canopy gradients as described in the supplement. Vertical gradients of these compounds can  
13 be significant (up to 80% change in mixing ratios between 4 and 23 m), thus this correction is a  
14 necessary step towards accurately representing in-canopy reactivity.

15

## 16 **2.4 Model Calculations**

17 Detailed model calculations utilized the University of Washington Chemical Model (UWCM).  
18 This model incorporates a subset of the Master Chemical Mechanism (MCM) v3.2 (Jenkin et al.,  
19 1997;Saunders et al., 2003) with several updates and additional chemistry as detailed elsewhere  
20 (Wolfe and Thornton, 2011). Model setup is similar to that described by Kim et al. (2013) but  
21 with a few modifications. All input data are averaged to a 30-minute diel cycle. Constraints  
22 include all observations listed above and constant mixing ratios of 1770 ppbv for  $\text{CH}_4$  and 550  
23 ppbv for  $\text{H}_2$ . The MCM mechanism subset includes all reactions from oxidation of MBO,  
24 isoprene,  $\alpha$ -pinene,  $\beta$ -pinene, limonene, benzene, toluene, butadiene, acetaldehyde, propanal, n-  
25 butanal and methane. The simple MT mechanism of Wolfe and Thornton (2011) is used for  
26 camphene and a group of unspeciaded monoterpenes (the latter are assumed to have the same  
27 chemistry as  $\beta$ -pinene). Isomerization of first-generation isoprene peroxy radicals (Peeters and  
28 Müller, 2010;Peeters et al., 2009) is also included using measured rate coefficients for  
29 isomerization (Crouse et al., 2011) and subsequent loss of hydroperoxyaldehydes (Wolfe et al.,

1 2012); recall that isoprene is, however, a relatively minor contributor to VOC chemistry at this  
2 site. To account for cloud and forest cover, the ratio of in-canopy observed and MCM-calculated  
3  $J(\text{NO}_2)$  is used to generate a scaling factor, which is then applied to all MCM-parameterized  
4 photolysis frequencies. Some of our analysis below suggests that certain peroxy radicals may be  
5 sensitive to direct sunlight (Sect. 5.1); however, the attenuated light profile better represents  
6 photolytic sources of OH at the measurement location, and we use observations of this radical to  
7 test proposed mechanisms. Emissions and deposition are not explicitly considered, but an  
8 additional first-order loss process with a lifetime of 24 hours is given to all species to represent  
9 physical losses (deposition and advection/dilution) and prevent buildup of long-lived products.  
10 The model is initialized at midnight and integrated for three days with observational constraints  
11 updated every 30 minutes. Three days is sufficient to reach a diurnal steady state, and results are  
12 shown from the third day. Specific model scenarios are described in the appropriate sections.  
13 Uncertainties in model mixing ratios are estimated from observational uncertainties as described  
14 in the supplement.

15 Comparing model results with  $\text{HO}_2^*$  requires some assumptions regarding the  
16 contribution of organic peroxy radicals to this measurement. To first order, we assume that the  
17  $\text{HO}_2^*$  measurement includes  $\text{HO}_2$  and all first and second-generation  $\beta$ -hydroxyalkylperoxy  
18 radicals produced from OH oxidation of MBO, isoprene, monoterpenes, MVK, MACR,  
19 butadiene, benzene and toluene; specific radicals used are listed in Table S2.

20

21

### 22 **3 Observations**

23 The majority of peroxy radical measurements were collected during the final two weeks of the  
24 campaign (16 – 30 August). Figure S1 of the online supplement shows the full time series for  
25 peroxy radical mixing ratios, OH concentrations and meteorology. Meteorological conditions  
26 were warm and moderately dry (average mid-day temperature and relative humidity of  $24 \pm 2$  °C  
27 and  $27 \pm 9$  %), with scattered clouds and occasional rain after noon. Total peroxy radicals  
28 exhibited a regular diel cycle with daytime maxima of 100 to 180 pptv and nighttime minima of  
29 0 to 10 pptv, within the range of observations from several other forest sites (Cantrell et al.,

1 1992;Cantrell et al., 1993;Qi et al., 2005). HO<sub>2</sub>\* tends to track total peroxy radicals, though the  
2 ratio of HO<sub>2</sub>\* to total peroxy radicals (not shown) can vary significantly (from 0.4 to ~1)  
3 throughout the day. Daytime OH mixing ratios ranged from  $3 \times 10^6$  to  $10 \times 10^6$  molec cm<sup>-3</sup>,  
4 while nighttime values were typically below the instrument detection limit of  $5 \times 10^5$  molec cm<sup>-3</sup>.  
5 Due to the regularity of diel cycles at this site and intermittent temporal overlap for many  
6 observations, our analysis will focus mainly on average diel behavior. All times discussed below  
7 refer to local solar time.

8 The mean diel cycle of peroxy radicals (Fig. 1) displays several interesting features. After  
9 sunrise, HO<sub>2</sub>\* and HO<sub>2</sub> + RO<sub>2</sub> rise synchronously with both OH and O<sub>3</sub> photolysis frequency,  
10 consistent with photochemical sources. From 11:30 to 14:30, there is a sharp rise in HO<sub>2</sub>\* and  
11 HO<sub>2</sub> + RO<sub>2</sub> that exceeds the smoother diel cycle seen in OH concentrations. This maximum,  
12 along with the brief spike at ~15:30, are consistent daily features and not an averaging artifact. In  
13 the afternoon, the decay of HO<sub>2</sub>\* is similar to that of OH, while HO<sub>2</sub> + RO<sub>2</sub> exhibits a shoulder  
14 that persists until ~16:30.

15 Nighttime peroxy radicals are low but consistently above the PeRCIMS detection limit of  
16 2 pptv, with mean mixing ratios from midnight to 05:00 of  $4 \pm 2$  pptv and  $6 \pm 2$  pptv for HO<sub>2</sub>\*  
17 and HO<sub>2</sub> + RO<sub>2</sub>, respectively. Observations in at least one semi-polluted area have suggested that  
18 NO<sub>3</sub> (nitrate radical) and/or ozone-driven chemistry can drive significant nighttime peroxy  
19 radical production in the presence of alkenes (Andres-Hernandez et al., 2013). For the conditions  
20 of BEACHON, Fry et al. (2013) have demonstrated that the oxidation of monoterpenes by NO<sub>3</sub>  
21 chemistry can be a significant source of particulate organic nitrates. Thus, even though peroxy  
22 radical levels are low, they imply significant radical-driven processes occurring in the absence of  
23 sunlight.

24 Figure 2 presents diel cycles for other key observations. Data are averaged over the full  
25 campaign (August 1 – 31). Unfortunately, intermittent data gaps do not permit more refined data  
26 selection. Though the degree of coverage varies for different species, most observations  
27 demonstrate consistent patterns from day to day. The sharp early morning rise in NO<sub>x</sub> may be  
28 due to entrainment from aloft during the breakup of the nocturnal boundary layer (Seok et al.,  
29 2013) or surface emission (Alaghmand et al., 2011). The onset of this feature is synchronous  
30 with a rapid rise in ozone, likely attributable to the former mechanism. Observed daytime NO

1 mixing ratios of 100 – 150 pptv are typical for a rural continental site and are within a transition  
2 region where reactions with both NO and other peroxy radicals (HO<sub>2</sub> and RO<sub>2</sub>) are expected to  
3 contribute significantly to total peroxy radical loss. MBO and monoterpenes, the primary  
4 emissions of Ponderosa pine, dominate the reactive VOC budget. Methanol is also abundant at  
5 this site (Kaser et al., 2013b), but it is relatively inert. Oxidation products, including  
6 formaldehyde, glyoxal and PAN, build up throughout the day, peaking in the late afternoon and  
7 decaying at night due to deposition, thermal decomposition and other losses. OH reactivity, a  
8 measure of the total OH loss rate, maintains a fairly constant value of 6 – 7 s<sup>-1</sup> during the day and  
9 rises to as much 14 s<sup>-1</sup> at night.

10

#### 11 **4 Model Results**

12 Two initial model scenarios are considered. In the first simulation, all observations other than  
13 peroxy radicals are used to constrain the model (“base”), while in a second simulation OH is  
14 determined by the model (“ModOH”). Figure 3 compares model output with RO<sub>x</sub> observations  
15 for both scenarios, and additional model results are shown in the SI (Fig. S4). In the base case,  
16 total peroxy radicals are under-predicted throughout the day, with errors of up to a factor of 3 at  
17 midday. Un-constraining OH decreases mid-day modeled peroxy radicals by more than 50%.  
18 The diel cycle of modeled peroxy radicals closely tracks that of OH in both scenarios. The  
19 morning rise in modeled and measured peroxy radical mixing ratios differs by several hours,  
20 suggesting a role for processes other than OH-driven VOC oxidation in early morning  
21 production. Moreover, the model captures neither the strong mid-day maximum nor the  
22 afternoon shoulder. In the ModOH scenario, OH concentrations are under-predicted throughout  
23 the day. This missing OH is likely at least partly due to an under-prediction of HO<sub>2</sub>, which  
24 reduces the rate of OH production via (R4).

25 The relationship between OH and peroxy radicals is somewhat complicated by  
26 photochemical gradients and the role of vertical transport. Above the canopy, increased sunlight  
27 likely leads to more OH and thus more peroxy radicals, as demonstrated by a separate set of  
28 model runs constrained by above-canopy J(NO<sub>2</sub>) data (Fig. S5). Some of these radicals will be  
29 transported into the canopy, sustaining photochemistry amidst attenuated radiation. To our  
30 knowledge, there are no published data comparing within and above-canopy peroxy radical

1 levels; however, detailed 1-D canopy modeling results predict relatively minor gradients in HO<sub>2</sub>  
2 and total RO<sub>2</sub> at other forests (Bryan et al., 2012;Makar et al., 1999;Wolfe and Thornton,  
3 2011;Wolfe et al., 2011a). For example, Wolfe and Thornton (2011) calculate that peroxy radical  
4 mixing ratios change by less than 10% within a Ponderosa pine forest similar to that of  
5 BEACHON-ROCS. This may reflect the fact that decreased in-canopy production is balanced by  
6 downward mixing. Thus, model underestimates of peroxy radicals may be partly due to a  
7 missing source from downward transport, but only inasmuch as production and destruction rates  
8 vary between above and below-canopy environments. Moreover, the tight coupling of OH and  
9 HO<sub>2</sub> suggests that this phenomenon can be mostly accounted for by constraining OH to  
10 measurements. In this case, modeled peroxy radical mixing ratios are essentially independent of  
11 radiation (Fig. S5); in other words, OH-initiated chemistry is the dominant peroxy radical source  
12 in the model.

13 Under-prediction of OH reactivity could also lead to disagreement between modeled and  
14 measured peroxy radicals. Missing OH reactivity is a common feature of many studies in regions  
15 dominated by biogenic VOC (Lou et al., 2010;Edwards et al., 2013). A detailed analysis of OH  
16 reactivity at BEACHON–ROCS shows that measured species can only account for 41% of the  
17 total OH reactivity on average, with poorer agreement at night (Nakashima et al., 2014). In the  
18 current study, the model underestimates total measured OH reactivity by as much as 20% during  
19 the day and by 40 to 50% at night for both scenarios (Fig. S4). It is important to note that  
20 unmeasured VOC oxidation products comprise a substantial fraction (up to 45%) of the modeled  
21 OH reactivity, and the abundance of these compounds is highly sensitive to the assumed dilution  
22 rate of 1 day<sup>-1</sup> (Edwards et al., 2013). For example, increasing the “physical loss” lifetime (Sect.  
23 2.4) from 24 to 48 hours increases modeled OH reactivity by ~1 s<sup>-1</sup>. We must also be wary of in-  
24 canopy heterogeneity. OH reactivity was measured at 4m above the ground but likely exhibits a  
25 vertical gradient within the canopy (Mogensen et al., 2011). From PTRMS observations of MBO  
26 and monoterpenes at 1m and 4m (data not shown), we expect total OH reactivity to change by  
27 less than 10% between 4m and the peroxy radical measurement height of 1.6 m. Even with these  
28 caveats, modeled and measured OH reactivity agree to within 20% during the day, suggesting  
29 that the base model adequately represents the overall rate of OH-driven RO<sub>2</sub> production. This  
30 implies that other processes must also influence the peroxy radical budget.

1 Overall, modeled  $\text{HO}_2^*$  agrees somewhat better with observations than does total peroxy  
2 radicals, especially with OH constrained (Fig. 3c). Based on the above assumptions,  $\text{HO}_2$   
3 comprises 60 – 70% of the modeled  $\text{HO}_2^*$ , giving peak midday modeled  $\text{HO}_2$  mixing ratios of 25  
4 and 12 pptv for the base and ModOH cases, respectively (Fig. S4). Roughly 50 – 60% of total  
5 modeled  $\text{RO}_2$  is produced from alkene oxidation (Fig. 4) and thus predicted to be detected as  
6  $\text{HO}_2^*$ . The remainder, which we refer to as  $\text{RO}_2^*$ , can be compared with observations by taking  
7 the difference between measured  $\text{HO}_2 + \text{RO}_2$  and  $\text{HO}_2^*$  (Fig. 3d).  $\text{RO}_2^*$  is generally  
8 underestimated, especially in the afternoon where the “shoulder” from  $\text{HO}_2 + \text{RO}_2$  appears as a  
9 distinct peak. This feature is an important clue regarding the nature of missing  $\text{RO}_2$ .

10 The distribution of  $\text{RO}_2$  radicals in the model closely follows that of VOC precursors  
11 (Fig. 4). MBO-derived  $\text{RO}_2$  are the most abundant component during the day, while nighttime  
12 chemistry is dominated by monoterpenes, particularly  $\beta$ -pinene and limonene. This trend occurs  
13 for two reasons. First, MBO emissions are dependent upon both light and temperature (Harley et  
14 al., 1998), while monoterpene emissions at this site scale primarily with temperature (Kaser et  
15 al., 2013a), leading to different diel cycles in their concentrations (Fig. 2b). Secondly, MBO  
16 reacts almost exclusively with OH, while monoterpenes are reactive towards OH,  $\text{O}_3$  and the  
17 nitrate radical ( $\text{NO}_3$ ). The latter oxidant typically only accumulates at night (Fry et al., 2013).  
18 Our model results indicate similar contributions from OH and  $\text{NO}_3$  chemistry to monoterpene  
19 oxidation in the first half of the night, with OH-driven loss prevailing in the early morning as  
20  $\text{NO}_3$  decays alongside its precursor, ozone. “Secondary”  $\text{RO}_2$  arising from oxidation of  
21 unmeasured VOC comprise as much as 49% of modeled  $\text{RO}_2$ , consistent with our earlier  
22 discussion of OH reactivity.  $\text{HO}_2$  comprises 35 – 50% of the total peroxy radical budget (Fig. 4).  
23 The diel cycle of  $\text{HO}_2/(\text{HO}_2 + \text{RO}_2)$  is essentially the same for both model scenarios,  
24 demonstrating that absolute OH concentrations influence peroxy radical abundances but not  
25 partitioning. The mid-day minimum in this ratio reflects the increased importance of (R8) as a  
26 sink of  $\text{HO}_2$  (see also Fig. 6).

27 In theory, model results can be used to estimate the contribution of  $\text{HO}_2$  to  $\text{HO}_2^*$   
28 observations. Several potential approaches are discussed in the SI. All of these methods  
29 inherently assume that model output faithfully represents the true peroxy radical distribution;  
30 however, without additional constraints on the nature of “missing” peroxy radicals, it is difficult

1 to judge the reliability of this assumption. Thus, we elect to focus our analysis on the measured  
2 quantities, HO<sub>2</sub>\* and RO<sub>2</sub>\*.

3

## 4 **5 Analysis and Discussion**

5 Modeled and observed peroxy radicals agree to within their respective uncertainties for much of  
6 the day (Fig. 3). Clear systematic discrepancies between average mixing ratios, however, suggest  
7 that the model is missing or misrepresenting sources and/or sinks of these species. Two features  
8 that stand out are the large midday maximum and the afternoon “shoulder,” neither of which are  
9 captured by the model. Figure 5 quantifies this measurement-model mismatch. The magnitude of  
10 the model-measurement discrepancy should be interpreted with caution, as the combined  
11 uncertainties from model and observations leads to uncertainties of as much as a factor of 2 in  
12 the difference. Most of this uncertainty is systematic in nature (e.g. accuracy of calibrations),  
13 thus we have somewhat more confidence in the diurnal pattern of these differences. Interestingly,  
14 most of the under-prediction in HO<sub>2</sub>\* arises from the midday maximum and the sharp afternoon  
15 satellite peak (Fig. 1), while RO<sub>2</sub>\* under-prediction persists throughout the day and includes  
16 most of the broad afternoon shoulder. These features allude to multiple mechanistic issues, and  
17 we examine each observation separately.

18

### 19 **5.1 Missing HO<sub>2</sub>\*: A Photolytic HO<sub>2</sub> Source?**

20 Understanding the nature of the midday HO<sub>2</sub>\* maximum requires that we first determine whether  
21 this peak is primarily due to changes in HO<sub>2</sub> or RO<sub>2</sub>. Given that 1) RO<sub>2</sub>\* does not display a  
22 similar feature, and 2) we expect most RO<sub>2</sub> to exhibit similar diel cycles (Fig. 4), additional HO<sub>2</sub>  
23 production is the simplest explanation. Production of specific RO<sub>2</sub> that contribute to HO<sub>2</sub>\*, such  
24 as from photolysis of some yet-unidentified VOC, is also possible but less likely. This hypothesis  
25 implies several testable consequences, as detailed below.

26 To gauge the magnitude of this putative HO<sub>2</sub> source, we first examine the rates of HO<sub>2</sub>  
27 production and loss calculated from the 0-D model (Fig. 6). Reaction of RO<sub>2</sub> with NO comprises  
28 ~60% of the modeled HO<sub>2</sub> source, with smaller contributions from photolysis and OH-reaction

1 of oxidized VOC (mainly formaldehyde, HCHO). NO chemistry also dominates the loss of HO<sub>2</sub>,  
2 though model underestimates of peroxy radical concentrations likely lead to an underestimate in  
3 the loss rates from reaction with HO<sub>2</sub> and RO<sub>2</sub>. We can quantify the “missing” production rate by  
4 assuming that HO<sub>2</sub> is in steady state and calculating the loss rate of the missing HO<sub>2</sub>:

$$5 \quad P_{miss} = L_{miss} = [HO_2^*]_{miss} / \tau_{HO_2, mod} \quad (1)$$

6 Here,  $[HO_2^*]_{miss}$  is the concentration of missing HO<sub>2</sub>\* (Fig. 5) and  $\tau_{HO_2, mod}$  is the lifetime of HO<sub>2</sub>  
7 calculated from the base model scenario. At its peak, the missing production rate is nearly double  
8 the total production rate from all known sources (Fig. 6, black line). For perspective, the  
9 maximum missing production rate of 102 ppt/min is 8 times the HO<sub>2</sub> production rate from  
10 reaction of MBO-derived RO<sub>2</sub> with NO and 24 times the production rate from HCHO photolysis.  
11 Reducing the HO<sub>2</sub> lifetime to account for under-predicted reaction rates with HO<sub>2</sub> and RO<sub>2</sub>  
12 (estimated using total peroxy radical measurements and the modeled HO<sub>2</sub>/RO<sub>2</sub> ratio) increases  
13  $P_{miss}$  by less than 20%.

14 Increased HO<sub>2</sub> will provide an additional source of OH. Thus, as a further test, we  
15 incorporate this extra HO<sub>2</sub> source as an additional 0<sup>th</sup>-order reaction in the ModOH scenario and  
16 compare model-calculated OH with observations (Fig. 7). This modification significantly  
17 increases daytime OH concentrations. Modeled OH generally agrees with observations (to within  
18 combined uncertainties) in the morning and afternoon hours but is over-predicted in the early  
19 afternoon, concomitant with the sharp HO<sub>2</sub>\* maximum. The overall model-measurement  
20 agreement improves (slope = 0.25 vs 1.19, Fig. 7(b)), but the correlation degrades somewhat ( $r^2$   
21 = 0.81 vs. 0.75). These results suggest that such an HO<sub>2</sub> radical source cannot be invoked  
22 without additional changes to the mechanism. Over-prediction of OH at the peak of extra HO<sub>2</sub>  
23 production likely indicates that some fraction of the missing HO<sub>2</sub>\* is actually RO<sub>2</sub>, counter to the  
24 simple assumption made above. Again, we caution that the magnitude of this missing HO<sub>2</sub>\*  
25 source is highly uncertain. Furthermore, these results support the conclusion of Kim et al. (2013)  
26 that HO<sub>2</sub> can be a major source of OH in the canopy environment.

27 A closer analysis of the observational dataset provides further characterization of the  
28 missing source. Figure 8 shows an example of the relationship between peroxy radicals and solar  
29 radiation on August 22; similar correlations were observed on many days of the campaign. Cloud  
30 cover regularly reduces direct sunlight at this site, decreasing above-canopy J(NO<sub>2</sub>) by factors of



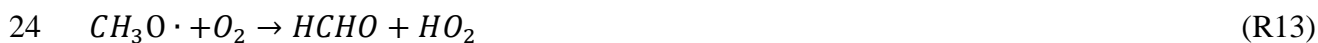
1 2 to 4. Cloud effects on  $J(\text{NO}_2)$  measured near the ground are comparatively minor since most of  
2 the radiation here is a combination of scattered diffuse light and occasional sun flecks (i.e. direct  
3 sun). In-canopy  $J(\text{NO}_2)$  is a factor of 3 to 6 lower than above-canopy clear sky values (Fig. S5);  
4 we again caution that this is not necessarily representative of the “average” in-canopy  
5 environment (Sect. 2.3). Indeed, the results in Fig. 8 suggest that direct sunlight penetrates much  
6 of the overstory throughout mid-day. This is consistent with our expectations for this relatively  
7 open canopy (LAI = 1.14, tree coverage = 38%).  $\text{HO}_2^*$  increases to ~80 pptv from 11:30 to  
8 14:30, consistent with the midday maximum in the diel average; however,  $\text{HO}_2^*$  also decreases  
9 rapidly during periods of sustained radiation attenuation, down to levels similar to those  
10 observed before and after the maximum.  $\text{RO}_2^*$  exhibits some correlation with above-canopy  
11 radiation (e.g. the troughs at hours 12:40 and 15:00), but generally the correlation is weaker and  
12 variations in  $\text{RO}_2^*$  are more independent of radiation. These trends are also borne out in the  
13 broader statistics of the full dataset (Fig. S7). The difference in the radiation dependence of  
14  $\text{HO}_2^*$  and  $\text{RO}_2^*$  suggests that fast changes in  $\text{HO}_2^*$  are not solely driven by the radiation  
15 dependence of OH.

16 The simplest explanation for the observed behavior is production of peroxy radicals from  
17 gas-phase oxidation and/or photolysis of VOC. Additional production from OH chemistry is  
18 unlikely, as the model is constrained by measured OH and reproduces observed OH reactivity to  
19 within 20% during the day (Fig. S4). Only a handful of VOC are known to exclusively produce  
20  $\text{HO}_2$  during OH oxidation, notably formaldehyde (HCHO) and glyoxal (HCOCHO), both of  
21 which are constrained by observations in our model. Gas-phase photolysis of an unidentified  
22 compound is another potential explanation, though the emission (or production) of such a  
23 molecule would need to match the unique profile of the  $\text{HO}_2^*$  midday maximum (Fig. 5). None  
24 of the other 213 meteorological and chemical observations resemble this profile, thus we have no  
25 additional clues as to the nature of this source.  $\text{HO}_2$  production from reactions of “missing”  $\text{RO}_2^*$   
26 with NO may also explain some of the missing  $\text{HO}_2^*$ , but not the mid-day maximum (see Sect.  
27 5.2 and Fig. 11).

28 Numerous investigations have inferred the presence of significant unidentified reactive  
29 hydrocarbons in biogenic environments. Often this conclusion arises from discrepancies between  
30 measured and calculated OH reactivity (Di Carlo et al., 2004; Lou et al., 2010; Sinha et al.,

1 2010;Mogensen et al., 2011;Nölscher et al., 2012;Edwards et al., 2013). It is still debated  
 2 whether the missing reactivity is due to primary emissions or secondary oxidation products,  
 3 though this likely varies from site to site. While under-represented OH reactivity could have a  
 4 profound impact on peroxy radical chemistry elsewhere, we reiterate that this is likely not a  
 5 viable explanation for missing peroxy radicals in the present study. Fast downward ozone fluxes  
 6 (Goldstein et al., 2004;Kurpius and Goldstein, 2003) and high levels of oxidized VOC  
 7 (Holzinger et al., 2005) have also been taken as evidence for unconventional in-canopy  
 8 chemistry. Both of these findings originate from observations in a Ponderosa pine ecosystem  
 9 similar to Manitou Experimental Forest, thus it is conceivable that similar chemistry is at play.  
 10 Perhaps the most relevant line of evidence for the present study is the observation of  
 11 unexpectedly large upward fluxes of HCHO during BEACHON-ROCS (DiGangi et al., 2011).  
 12 Formaldehyde is a major product from the oxidation of nearly every VOC and is thus an  
 13 excellent tracer for the overall efficiency of hydrocarbon degradation. DiGangi et al. (2011)  
 14 demonstrated that a simple mass balance model incorporating known chemical and physical  
 15 processes under-predicted the observed HCHO flux by a factor of 6. The investigators concluded  
 16 that the missing HCHO source could be attributed to oxidation of unidentified biogenic VOC  
 17 and/or direct emissions of HCHO from vegetation. In either case, closure of the HCHO flux  
 18 budget required that the missing process correlate with solar radiation.

19 It is possible that the missing sources of HCHO and HO<sub>2</sub>\* are related. The maximum  
 20 “missing” HCHO flux of ~20 pptv m/s corresponds to an in-canopy HCHO production rate of 65  
 21 pptv/min (for a canopy height of 18.5 m), within the range of the missing HO<sub>2</sub>\* source (Fig. 6).  
 22 Candidate precursors for both HCHO and HO<sub>2</sub> are methylperoxy, hydroxymethyl and β-  
 23 hydroxyalkoxy radicals, which decompose rapidly under normal atmospheric conditions:



27 The lifetimes of these radicals are so short that the above reactions are often assumed to be  
 28 instantaneous. In conventional chemical mechanisms, these radicals are intermediates of peroxy  
 29 radical decomposition (mainly via reaction with NO). While known photolytic sources for such

1 molecules are thought to be minor, it is possible that photolysis of yet-unidentified VOC could  
2 simultaneously stimulate production of both HCHO and HO<sub>2</sub>, which in turn would accelerate  
3 HO<sub>x</sub>-driven photochemistry within and above the forest canopy.

4

## 5 **5.2 Missing RO<sub>2</sub>\*: Evidence for Unidentified VOC?**

6 In contrast to HO<sub>2</sub>\*, missing RO<sub>2</sub>\* mixing ratios exhibit a relatively smooth diel cycle (Fig. 5).  
7 This signal comprises most of the total missing peroxy radicals in the morning and afternoon,  
8 with a maximum at ~16:00. The shape of the diel profile is notably similar to that of several  
9 oxidation products, including HCHO, glyoxal and PAN (Fig. 2(c)). Many modeled oxidation  
10 products, including first-generation peroxides and organic nitrates, also peak at this time (not  
11 shown). RO<sub>2</sub> sinks are dominated by reaction with NO (Fig. 9), and under-prediction of HO<sub>2</sub> in  
12 the base simulation likely results in under-estimation of RO<sub>2</sub> loss via reaction with HO<sub>2</sub>. Thus,  
13 missing RO<sub>2</sub>\* reflects an issue with RO<sub>2</sub> sources.

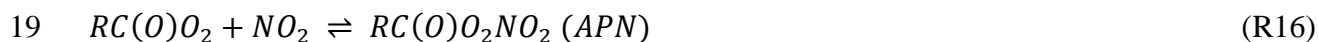
14 We can estimate the magnitude of the missing RO<sub>2</sub>\* source using an approach similar to  
15 that described for HO<sub>2</sub>\* (Eq. (1)). This method requires calculation of the missing RO<sub>2</sub>\* lifetime;  
16 however, this value depends on the assumed structure of these peroxy radicals. Figure 9(a)  
17 illustrates this point for three representative peroxy radicals. The lifetime of CH<sub>3</sub>O<sub>2</sub> and  
18 MBOAO<sub>2</sub> (the primary RO<sub>2</sub> from MBO oxidation) ranges from 30 to 60 seconds throughout the  
19 day, except in the morning when NO concentrations spike. In contrast, the lifetime of the acetyl  
20 peroxy radical, CH<sub>3</sub>CO<sub>3</sub>, is typically < 20 seconds. These differences arise mainly from NO  
21 reaction rate constants, which are 7.7, 9.0 and 20 x 10<sup>-12</sup> cm<sup>3</sup> molec<sup>-1</sup> s<sup>-1</sup> at 298 K for CH<sub>3</sub>O<sub>2</sub>,  
22 MBOAO<sub>2</sub> and CH<sub>3</sub>CO<sub>3</sub>, respectively. Figure 9(a) also shows the concentration-weighted  
23 average RO<sub>2</sub>\* lifetime for all model species in the RO<sub>2</sub>\* group. Coincidentally, this lifetime is  
24 nearly identical to that of MBOAO<sub>2</sub> even though this radical is not included in RO<sub>2</sub>\*.

25 Figure 9(b) compares the total production rate of modeled RO<sub>2</sub>\* with missing RO<sub>2</sub>\*  
26 production rates as calculated via the RO<sub>2</sub>\*-equivalent of Eq. (1). The magnitude of the missing  
27 production rate is similar to that of the “known” production rate except when RO<sub>2</sub>\* is assumed to  
28 have a lifetime comparable to CH<sub>3</sub>CO<sub>3</sub>. For the other three cases, missing RO<sub>2</sub>\* production  
29 follows a diurnal pattern similar to its concentration profile (Fig. 5c) except in the morning,

1 where the steady-state assumption may be invalid due to rapidly-changing NO concentrations.  
2 Recall that the absolute magnitude of this source is dependent on our estimate of missing RO<sub>2</sub>\*  
3 and thus is highly uncertain.

4 The contrast between diurnal cycles of production rates for “known” and missing RO<sub>2</sub>\*  
5 (Fig. 9b) demonstrates that the processes driving missing RO<sub>2</sub>\* are not solely sun-driven (i.e. OH  
6 reaction with VOC). Figure 10 shows modeled tendencies for the same three representative RO<sub>2</sub>  
7 species (MBOAO<sub>2</sub>, CH<sub>3</sub>O<sub>2</sub> and CH<sub>3</sub>CO<sub>3</sub>). Overall radical production tends to track with solar  
8 radiation, but some processes exhibit minor diurnal asymmetry. In particular, production of  
9 CH<sub>3</sub>O<sub>2</sub> and CH<sub>3</sub>CO<sub>3</sub> radicals from reactions of other RO<sub>2</sub> with NO maximizes slightly after noon  
10 due to both an increase in NO (Fig. 2(a)) and the buildup of RO<sub>2</sub>. Despite these features, OH is  
11 still the main driver for classical RO<sub>2</sub> production, and none of the 347 modeled RO<sub>2</sub> species  
12 exhibit a profile similar to that of the missing RO<sub>2</sub>\*. While amplification of a purely OH or light-  
13 dependent process may be able to explain missing RO<sub>2</sub>\* in the morning, such a source cannot  
14 explain the afternoon maximum. These results lead us to consider other non-OH RO<sub>2</sub> sources  
15 that may be under-represented in the model mechanism.

16 One potential candidate for missing RO<sub>2</sub>\* is the acyl peroxy (AP) radical family. AP  
17 radicals are a special class of peroxy radical that can react with NO<sub>2</sub> to form a metastable acyl  
18 peroxy nitrate (APN):



20 Temperature controls the lifetime of APNs; for the conditions of BEACHON-ROCS (4 to 29  
21 °C), the lifetime of PAN ranges from 23 hours to 24 minutes. APNs can act as a source or sink of  
22 AP radicals depending on equilibrium conditions and the strength of primary AP sources  
23 (LaFranchi et al., 2009). Our model predicts that PAN, the most abundant APN, is a net sink for  
24 acetyl peroxy radicals (Fig. 10(c)); however, the net rate of CH<sub>3</sub>CO<sub>3</sub> loss via PAN formation is  
25 small compared to primary CH<sub>3</sub>CO<sub>3</sub> production and reaction with NO, indicating near-steady  
26 state conditions (Cleary et al., 2007; LaFranchi et al., 2009). Moreover, the model predicts a  
27 number of additional APNs, with PAN (which is constrained by observations) comprising only  
28 19 – 39% of the total budget. The next most abundant APN is the MCM species C4PAN5, a  
29 byproduct of MBO oxidation, at 17 – 22%. The shape of the missing RO<sub>2</sub>\* profile may imply an

1 under-estimation in the source of AP radicals from decomposition of such APNs. Assuming  
2 steady state conditions for APNs, the AP radical concentration from this source alone is given by

$$3 \quad [AP] = \frac{k_{16r}[APN]}{k_{16f}[NO_2]} \quad (2)$$

4 where  $k_{16r}$  and  $k_{16f}$  are the reverse and forward rate constants for reaction (R16). Based on this  
5 equation, errors in APN concentrations and/or reaction rates could lead to under-prediction of AP  
6 radicals. Errors in APN concentrations are likely not a viable explanation. Evidence from other  
7 investigations suggests that >90% of the total peroxy nitrate budget is comprised of only a  
8 handful of APNs, mostly PAN (Wooldridge et al., 2010); thus, it is likely that modeled APN  
9 concentrations are already over-estimated. Errors in rate constants are more probable, as MCM  
10 rate constants for APN formation and loss are assumed equal to that of PAN, except for  
11 decomposition of PPN and MPAN, which follow IUPAC recommendations (Jenkin et al.,  
12 1997;Saunders et al., 2003). Laboratory data from Kirchner et al. (1999) indicate that  
13 decomposition rates generally decrease with increasing size and decreasing electronegativity of  
14 the organic functional group. In contrast, IUPAC recommends decomposition rate constants for  
15 PPN and MPAN that are ~10% faster than that of PAN. Formation rate constants have not been  
16 measured for species other than PAN, though one study has suggested that PPN formation may  
17 be 11% slower than that of PAN (Sommariva et al., 2011). To completely explain missing  $RO_2^*$ ,  
18 we estimate that the equilibrium constant ( $k_{18f}/k_{18r}$ ) for model APNs would need to decrease by  
19 more than a factor of 10, well beyond the likely uncertainty in this value. Moreover, model  
20 simulations show that most of the growth in the  $RO_2$  pool from such a change is due not to AP  
21 radicals themselves but rather to the  $RO_2$  products of the reaction of AP with NO. Thus, we  
22 conclude that AP radicals are not a major component of missing  $RO_2^*$ .

23 Other  $RO_2^*$  generation mechanisms to consider include reaction of VOC with ozone or  
24 nitrate radical ( $NO_3$ ). In the base model simulation, ozone chemistry contributes 10 – 20% to the  
25 daytime peroxy radical budget, while  $NO_3$  chemistry is only significant at night. Ozonolysis of  
26 unidentified VOC has been invoked previously to explain anomalously high ozone fluxes  
27 (Goldstein et al., 2004;Hogg et al., 2007;Kurpius and Goldstein, 2003), oxidation product  
28 concentrations (Holzinger et al., 2005) and sulfuric acid levels (Mauldin et al., 2012) in other  
29 forests. Decomposition of Criegee intermediates can simultaneously generate OH and  $RO_2$   
30 radicals, with measured yields ranging from 0.06 to near-unity (Aschmann et al., 2002;Atkinson

1 and Arey, 2003;Shu and Atkinson, 1994). In a detailed modeling study, Wolfe et al. (2011b)  
2 established an upper limit for RO<sub>2</sub> production from ozonolysis of “very reactive” VOC of 60  
3 pptv min<sup>-1</sup>, similar to both our missing RO<sub>2</sub>\* source and the missing HCHO source inferred by  
4 DiGangi et al. (2011). The latter study also determined that any missing VOC should exhibit a  
5 light-dependent emission profile similar to that of MBO.

6 To test this hypothesis, we implement an additional set of reactions following the very  
7 reactive VOC mechanism described by Wolfe et al. (2011b). Specific reactions are listed in  
8 Table S3. Rate constants for initial oxidation of this hypothetical VOC are assumed equal to  
9 those of β-caryophyllene, while reactions of the peroxy radical products are assumed to be  
10 similar to those of the β-pinene-derived radical BPINAO2. As a modification to the original  
11 mechanism, we discriminate between RO<sub>2</sub> made by OH, O<sub>3</sub> and NO<sub>3</sub> chemistry, since we  
12 anticipate that OH-derived RO<sub>2</sub> would be detected as HO<sub>2</sub>\* in the PeRCIMS inlet. The yield of  
13 OH and RO<sub>2</sub> from ozonolysis is set to the upper limit of 0.1 recommended by Wolfe et al.  
14 (2011b). Very reactive VOC mixing ratios, shown in Fig. S8, are fixed to a diurnal cycle that  
15 scales with the observed flux of the sum of MBO and isoprene (Kaser et al., 2013a). The scaling  
16 factor of 0.23 is chosen to optimize model-measurement agreement for total peroxy radicals in  
17 the base scenario. We caution that inferred VRVOC mixing ratios depend directly on the  
18 assumed reaction rate constants and product yields – the product of which determines the RO<sub>2</sub>  
19 production rate. In other words, this calculation effectively constrains the VRVOC reactivity, as  
20 discussed in Wolfe et al. (2011b). For these conditions, modeled OH reactivity increases by as  
21 much as 30%.

22 We implement this mechanism for both the base and ModOH scenarios; results are  
23 shown in Figure 11. Model-measurement agreement for all radicals improves markedly on  
24 incorporating very reactive VOC chemistry (compare to Fig. 3), though the unique diurnal  
25 patterns of HO<sub>2</sub>\* and RO<sub>2</sub>\* are not captured. With OH constrained to observations, model  
26 agreement with HO<sub>2</sub>\* improves due to 1) RO<sub>2</sub> from reaction of very reactive VOC with OH and  
27 2) increased HO<sub>2</sub> from reaction of new RO<sub>2</sub> radicals with NO. With OH determined by the  
28 model, however, HO<sub>2</sub>\* is over-predicted in the afternoon. This is mainly driven by excess OH  
29 co-produced with RO<sub>2</sub> during ozonolysis of very reactive VOC. On the other hand, the latter  
30 fraction of RO<sub>2</sub> also improves agreement with RO<sub>2</sub>\*. Thus, the ozonolysis of unidentified

1 hydrocarbons alone cannot provide closure of the  $RO_x$  budget unless 1) OH is not produced with  
2 the same yield as  $RO_2$ , contrary to canonical mechanisms, or 2) additional processes are invoked  
3 that affect the diel OH profile. Nonetheless, these results strongly support an intimate chemical  
4 link between missing peroxy radicals and other yet-unexplained observations (i.e. HCHO and  
5 ozone fluxes) within the canopy airspace.

6

## 7 **6 Conclusions**

8 Using the comprehensive suite of observations from the 2010 BEACHON-ROCS field  
9 campaign, we have explored the detailed chemistry of peroxy radicals in a rural environment  
10 dominated by biogenic hydrocarbons. Total peroxy radical concentrations are among the highest  
11 yet reported, exceeding 100 pptv on every day of observations and reaching as high as 180 pptv.  
12 Box model calculations under-predict total peroxy radicals by as much as a factor of 3, indicative  
13 of missing sources. Though the PeRCIMS instrument does not provide a strict segregation  
14 between  $HO_2$  and  $RO_2$  radicals, the data alludes to several distinct sources. High levels of  $HO_2^*$   
15 at mid-day, combined with a clear dependence on radiation and a lack of similar behavior in  
16  $RO_2^*$ , suggest a missing photolytic source of  $HO_2$ . The magnitude of this missing source is  
17 highly uncertain, and its exact nature remains a mystery.  $RO_2^*$  is also under-predicted, but the  
18 diel profile of missing  $RO_2^*$  more closely resembles that of oxidation products and light-  
19 dependent VOC emissions. Implementing an additional chemical mechanism involving  
20 ozonolysis of putative “very reactive” VOC greatly improves model-measurement agreement  
21 with all radicals. With OH determined by the model, this same mechanism degrades agreement  
22 with measured OH and  $HO_2^*$  unless the OH yield is assumed to be lower than the  $RO_2$  yield,  
23 contrary to classical chemistry. While these results do not provide closure of the radical budget,  
24 they do imply that similar mechanisms may underlie both missing peroxy radicals and other  
25 indicators of faster-than-expected chemistry at this and other forests.

26 Failure to accurately represent peroxy radical chemistry in biogenic regimes will limit the  
27 reliability of model results and predictions. For example, the impact of peroxy radicals on ozone  
28 production is a complex balance between the NO turnover rate and the production of radical  
29 reservoirs, such as alkyl nitrates and peroxy acyl nitrates. Modeled production of such  
30 compounds depends directly on the calculated  $RO_2$  distribution, and changing the assumed yield

1 of NO<sub>x</sub> reservoir species can alter ozone production on regional and larger scales (Farmer et al.,  
2 2011;Paulot et al., 2012). Inter-conversion of reactive nitrogen also affects estimates of nitrogen  
3 deposition, which represents a critical link between atmospheric composition and ecosystem  
4 health (Sparks et al., 2008). Peroxy radical chemistry is also intimately tied to atmospheric  
5 oxidizing capacity. In environments where HO<sub>2</sub> is a dominant precursor of OH, missing peroxy  
6 radical sources will lead to underestimation of the overall rate of oxidation. Understanding this  
7 chemistry is particularly critical in high-VOC, low-NO<sub>x</sub> regimes where radical cycling is  
8 controlled by RO<sub>x</sub> + HO<sub>2</sub> reactions and, potentially, unimolecular decomposition of larger RO<sub>2</sub>  
9 (Archibald et al., 2010;Stavrakou et al., 2010). For all these reasons, it is imperative that we  
10 identify and eliminate remaining gaps in our understanding of chemistry in such environments –  
11 especially if mechanistic shortcomings are as substantial as implied by this study.

12 Closure of the RO<sub>x</sub> budget will require a comprehensive understanding of both primary  
13 radical sources and the processes that control radical cycling in the continental boundary layer.  
14 Of critical importance is continued measurement of organic peroxy radicals, as these are too  
15 often a key missing constraint in modeling studies. Further speciation of these compounds would  
16 also greatly aid identification of errors in current chemical mechanisms. While it may not yet be  
17 technically feasible to segregate all individual RO<sub>2</sub>, progress could be made by determining the  
18 distribution of different RO<sub>2</sub> families (i.e. acyl peroxy, β-hydroxyalkylperoxy, etc.) (Whalley et  
19 al., 2013b). Measurements of radical reservoirs and termination products, such as organic  
20 peroxides (ROOH) and alkyl nitrates (RONO<sub>2</sub>), will also play a vital role in this regard.  
21 Observations of total ozone production (Cazorla and Brune, 2010) may also provide a useful  
22 check on observations of total peroxy radical concentrations while offering an integrated  
23 perspective on pertinent chemistry in biogenic environments. Finally, detailed comparisons of  
24 regional-scale chemical transport models with in situ chemical observations and derived  
25 properties (e.g. ozone production) are needed for full evaluation of the impact of mechanistic  
26 uncertainties on current and future predictions of atmospheric composition and air quality.

27

## 28 **Acknowledgements**

29 The National Center for Atmospheric Research is operated by the University Corporation for  
30 Atmospheric Research under sponsorship from the US National Science Foundation. Any



1 opinions, findings and conclusions or recommendations expressed in this publication are those of  
2 the authors and do not necessarily reflect the views of the National Science Foundation. The  
3 authors also thank the National Science Foundation (ATM 0852406) and the Austrian Science  
4 Fund (FWF) under the project number L518-N20. Lisa Kaser is a recipient of a DOC-fFORTE-  
5 fellowship of the Austrian Academy of Sciences at the Institute of Ion Physics and Applied  
6 Physics. This work was also supported by the EC Seventh Framework Program (Marie Curie  
7 Reintegration Program, “ALP-AIR”, grant no. 334084) to TK. GMW acknowledges support  
8 from the NOAA Climate and Global Change Postdoctoral Fellowship Program. We thank the US  
9 Forest Service, specifically Richard Oakes, for logistical support during BEACHON. Finally, we  
10 a grateful for the insightful comments of 3 anonymous referees.

11

## 12 **References**

- 13 Alaghmand, M., Shepson, P. B., Starn, T. K., Jobson, B. T., W., W. H., Carroll, M. A., Bertman, S. B., Lamb,  
14 B., Edburg, S. L., Zhou, X., Apel, E., Riemer, D., Stevens, P., and Keutsch, F.: The Morning NO<sub>x</sub>  
15 maximum in the forest atmosphere boundary layer, *Atmospheric Chemistry and Physics Discussions*,  
16 11, 29251-29282, 10.5194/acpd-11-29251-2011, 2011.
- 17 Andres-Hernandez, M. D., Kartal, D., Crowley, J. N., Sinha, V., Regelin, E., Martinez-Harder, M.,  
18 Nenakhov, V., Williams, J., Harder, H., Bozem, H., Song, W., Thieser, J., Tang, M. J., Beigi, Z. H., and  
19 Burrows, J. P.: Diel peroxy radicals in a semi-industrial coastal area: nighttime formation of free  
20 radicals, *Atmospheric Chemistry and Physics*, 13, 5731-5749, 10.5194/acp-13-5731-2013, 2013.
- 21 Archibald, A. T., Cooke, M. C., Utembe, S. R., Shallcross, D. E., Derwent, R. G., and Jenkin, M. E.: Impacts  
22 of mechanistic changes on HO<sub>x</sub> formation and recycling in the oxidation of isoprene, *Atmos. Chem.*  
23 *Phys.*, 10, 8097-8118, 2010.
- 24 Aschmann, S. M., Arey, J., and Atkinson, R.: OH radical formation from the gas-phase reactions of O<sub>3</sub>  
25 with a series of terpenes, *Atmos. Environ.*, 36, 4347-4355, 2002.
- 26 Atkinson, R., and Arey, J.: Atmospheric degradation of volatile organic compounds, *Chem. Rev.*, 103,  
27 4605-4638, 2003.
- 28 Browne, E. C., and Cohen, R. C.: Effects of biogenic nitrate chemistry on the NO<sub>x</sub> lifetime in remote  
29 continental regions, *Atmos. Chem. Phys.*, 12, 11917-11932, 10.5194/acp-12-11917-2012, 2012.
- 30 Bryan, A. M., Bertman, S. B., Carroll, M. A., Dusanter, S., Edwards, G. D., Forkel, R., Griffith, S., Guenther,  
31 A. B., Hansen, R. F., Helmig, D., Jobson, B. T., Keutsch, F. N., Lefer, B. L., Pressley, S. N., Shepson, P.  
32 B., Stevens, P. S., and Steiner, A. L.: In-canopy gas-phase chemistry during CABINEX 2009: sensitivity  
33 of a 1-D canopy model to vertical mixing and isoprene chemistry, *Atmos. Chem. Phys.*, 12, 8829-  
34 8849, 10.5194/acp-12-8829-2012, 2012.
- 35 Cantrell, C. A., Lind, J. A., Shetter, R. E., Calvert, J. G., Goldan, P. D., Kuster, W., Fehsenfeld, F. C.,  
36 Montzka, S. A., Parrish, D. D., Williams, E. J., Buhr, M. P., Westberg, H. H., Allwine, G., and Martin, R.:

- 1 Peroxy-Radicals In The Rose Experiment - Measurement And Theory, *J. Geophys. Res. Atmos.*, 97,  
2 20671-20686, 1992.
- 3 Cantrell, C. A., Shetter, R. E., Calvert, J. G., Parrish, D. D., Fehsenfeld, F. C., Goldan, P. D., Kuster, W.,  
4 Williams, E. J., Westberg, H. H., Allwine, G., and Martin, R.: Peroxy Radicals as Measured in ROSE and  
5 Estimated From Photostationary State Deviations, *J. Geophys. Res.*, 98, 18355-18366, 1993.
- 6 Cantrell, C. A., Mauldin, L., Zondlo, M., Eisele, F., Kosciuch, E., Shetter, R., Lefer, B., Hall, S., Campos, T.,  
7 Ridley, B., Walega, J., Fried, A., Wert, B., Flocke, F., Weinheimer, A., Hannigan, J., Coffey, M., Atlas,  
8 E., Stephens, S., Heikes, B., Snow, J., Blake, D., Blake, N., Katzenstein, A., Lopez, J., Browell, E. V.,  
9 Dibb, J., Scheuer, E., Seid, G., and Talbot, R.: Steady state free radical budgets and ozone  
10 photochemistry during TOPSE, *Journal of Geophysical Research-Atmospheres*, 108, 22,  
11 10.1029/2002jd002198, 2003.
- 12 Carslaw, N., Creasey, D. J., Harrison, D., Heard, D. E., Hunter, M. C., Jacobs, P. J., Jenkin, M. E., Lee, J. D.,  
13 Lewis, A. C., Pilling, M. J., Saunders, S. M., and Seakins, P. W.: OH and HO<sub>2</sub> radical chemistry in a  
14 forested region of north-western Greece, *Atmos. Environ.*, 35, 4725-4737, 2001.
- 15 Cazorla, M., and Brune, W. H.: Measurement of Ozone Production Sensor, *Atmos. Meas. Tech.*, 3, 545-  
16 555, 10.5194/amt-3-545-2010, 2010.
- 17 Chacon-Madrid, H. J., and Donahue, N. M.: Fragmentation vs. functionalization: chemical aging and  
18 organic aerosol formation, *Atmos. Chem. Phys.*, 11, 10533-10563, 10.5194/acp-11-10553-2011,  
19 2011.
- 20 Cleary, P. A., Wooldridge, P. J., Millet, D. B., McKay, M., Goldstein, A. H., and Cohen, R. C.: Observations  
21 of total peroxy nitrates and aldehydes: measurement interpretation and inference of OH radical  
22 concentrations, *Atmos. Chem. Phys.*, 7, 1947-1960, 2007.
- 23 Crouse, J. D., Paulot, F., Kjaergaard, H. G., and Wennberg, P. O.: Peroxy radical isomerization in the  
24 oxidation of isoprene, *Phys. Chem. Chem. Phys.*, 13, 13607-13613, 2011.
- 25 Crouse, J. D., Knap, H. C., Ørnsø, K. B., Jørgensen, S., Paulot, F., Kjaergaard, H. G., and Wennberg, P. O.:  
26 On the atmospheric fate of methacrolein: 1. Peroxy radical isomerization following addition of OH  
27 and O<sub>2</sub>, *Journal of Physical Chemistry A*, 116, 5756-5762, 10.1021/jp211560u, 2012.
- 28 Crouse, J. D., Nielsen, L. B., Jørgensen, S., Kjaergaard, H. G., and Wennberg, P. O.: Autoxidation of  
29 Organic Compounds in the Atmosphere, *Journal of Physical Chemistry Letters*, 4, 3513-3520,  
30 10.1021/jz4019207, 2013.
- 31 da Silva, G., Graham, C., and Wang, Z. F.: Unimolecular beta-Hydroxyperoxy Radical Decomposition with  
32 OH Recycling in the Photochemical Oxidation of Isoprene, *Environ. Sci. Technol.*, 44, 250-256, 2010.
- 33 Di Carlo, P., Brune, W. H., Martinez, M., Harder, H., Leshner, R., Ren, X. R., Thornberry, T., Carroll, M. A.,  
34 Young, V., Shepson, P. B., Riemer, D., Apel, E., and Campbell, C.: Missing OH reactivity in a forest:  
35 Evidence for unknown reactive biogenic VOCs, *Science*, 304, 722-725, 2004.
- 36 DiGangi, J. P., Boyle, E. S., Karl, T., Harley, P., Turnipseed, A., Kim, S., Cantrell, C., Maudlin III, R. L., Zheng,  
37 W., Flocke, F., Hall, S. R., Ullmann, K., Nakashima, Y., Paul, J. B., Wolfe, G. M., Desai, A. R., Kajii, Y.,  
38 Guenther, A., and Keutsch, F. N.: First direct measurements of formaldehyde flux via eddy  
39 covariance: implications for missing in-canopy formaldehyde sources, *Atmos. Chem. Phys.*, 11,  
40 10565-10578, 2011.
- 41 DiGangi, J. P., Henry, S. B., Kammrath, A., Boyle, E. S., Kaser, L., Schnitzhofer, R., Graus, M., Turnipseed,  
42 A., Park, J.-H., Weber, R. J., Hornbrook, R. S., Cantrell, C., Maudlin III, R. L., Kim, S., Nakashima, Y.,

1 Wolfe, G. M., Kajii, Y., Apel, E. C., Goldstein, A. H., Guenther, A., Karl, T., Hansel, A., and Keutsch, F.  
2 N.: Observations of Glyoxal and Formaldehyde as Metrics for the Anthropogenic Impact on Rural  
3 Photochemistry, *Atmos. Chem. Phys.*, 12, 9529-9543, 10.5194/acp-12-9529-2012, 2012.

4 Dillon, T. J., and Crowley, J. N.: Direct detection of OH formation in the reactions of HO<sub>2</sub> with CH<sub>3</sub>C(O)O<sub>2</sub>  
5 and other substituted peroxy radicals, *Atmos. Chem. Phys.*, 8, 4877-4889, 2008.

6 Edwards, G. D., Cantrell, C. A., Stephens, S., Hill, B., Goyea, O., Shetter, R. E., Mauldin, R. L., Kosciuch, E.,  
7 Tanner, D. J., and Eisele, F. L.: Chemical ionization mass spectrometer instrument for the  
8 measurement of tropospheric HO<sub>2</sub> and RO<sub>2</sub>, *Anal. Chem.*, 75, 5317-5327, 2003.

9 Edwards, P. M., Evans, M. J., Furneaux, K. L., Hopkins, J., Ingham, T., Jones, C., Lee, J. D., Lewis, A. C.,  
10 Moller, S. J., Stone, D., Whalley, L. K., and Heard, D. E.: OH reactivity in a South East Asian tropical  
11 rainforest during the Oxidant and Particle Photochemical Processes (OP3) project, *Atmospheric  
12 Chemistry and Physics*, 13, 9497-9514, 10.5194/acp-13-9497-2013, 2013.

13 Faloon, I., Tan, D., Brune, W., Hurst, J., Barket, D., Couch, T. L., Shepson, P., Apel, E., Riemer, D.,  
14 Thornberry, T., Carroll, M. A., Sillman, S., Keeler, G. J., Sagady, J., Hooper, D., and Paterson, K.:  
15 Nighttime observations of anomalously high levels of hydroxyl radicals above a deciduous forest  
16 canopy, *J. Geophys. Res. Atmos.*, 106, 24315-24333, 2001.

17 Farmer, D. K., Perring, A. E., Wooldridge, P. J., Blake, D. R., Baker, A., Meinardi, S., Huey, L. G., Tanner, D.,  
18 O.Vargas, and Cohen, R. C.: Impact of organic nitrates on urban ozone production, *Atmos. Chem.  
19 Phys.*, 11, 4085-4094, 2011.

20 Fry, J. L., Draper, D. C., Zarzana, K. J., Campuzano-Jost, P., Day, D. A., Jimenez, J. L., Brown, S. S., Cohen,  
21 R. C., Kaser, L., Hansel, A., Cappellin, L., Karl, T., Hodzic Roux, A., Turnipseed, A., Cantrell, C., Lefer, B.  
22 L., and Grossberg, N.: Observations of gas- and aerosol-phase organic nitrates at BEACHON-RoMBAS  
23 2011, *Atmospheric Chemistry and Physics*, 13, 8585-8605, 10.5194/acp-13-8585-2013, 2013.

24 Fuchs, H., Bohn, B., Hofzumahaus, A., Holland, F., Lu, K. D., Nehr, S., Rohrer, F., and Wahner, A.:  
25 Detection of HO<sub>2</sub> by laser-induced fluorescence: calibration and interferences from RO<sub>2</sub> radicals,  
26 *Atmos. Meas. Tech.*, 4, 1209-1225, 2011.

27 Goldstein, A. H., McKay, M., Kurpius, M. R., Schade, G. W., Lee, A., Holzinger, R., and Rasmussen, R. A.:  
28 Forest thinning experiment confirms ozone deposition to forest canopy is dominated by reaction  
29 with biogenic VOCs, *Geophys. Res. Lett.*, 31, L22106, 10.1029/2004GL021259, 2004.

30 Griffith, S. M., Hansen, R. F., Dusanter, S., Stevens, P. S., Alaghmand, M., Bertman, S. B., Carroll, M. A.,  
31 Erickson, M., Galloway, M., Grossberg, N., Hottle, J., Hou, J., Jobson, B. T., Kamrath, A., Keutsch, F.  
32 N., Lefer, B. L., Mielke, L. H., O'Brien, A., Shepson, P. B., Thurlow, M., Wallace, W., Zhang, N., and  
33 Zhou, X. L.: OH and HO<sub>2</sub> radical chemistry during PROPHET 2008 and CABINEX 2009-Part 1:  
34 Measurements and model comparison, *Atmospheric Chemistry and Physics*, 13, 5403-5423,  
35 10.5194/acp-13-5403-2013, 2013.

36 Guenther, A. B., Jiang, X., Heald, C. L., Sakulyanontvittaya, T., Duhl, T., Emmons, L. K., and Wang, X.: The  
37 Model of Emissions of Gases and Aerosols from Nature version 2.1 (MEGAN2.1): an extended and  
38 updated framework for modeling biogenic emissions, *Geoscientific Model Development*, 5, 1471-  
39 1492, 10.5194/gmd-5-1471-2012, 2012.

40 Hallquist, M., Wenger, J. C., Baltensperger, U., Rudich, Y., Simpson, D., Claeys, M., Dommen, J., Donahue,  
41 N. M., George, C., Goldstein, A. H., Hamilton, J. F., Herrmann, H., Hoffmann, T., Iinuma, Y., Jang, M.,  
42 Jenkin, M. E., Jimenez, J. L., Kiendler-Scharr, A., Maenhaut, W., McFiggans, G., Mentel, T. F., Monod,  
43 A., Prevot, A. S. H., Seinfeld, J. H., Surratt, J. D., Szmigielski, R., and Wildt, J.: The formation,

1 properties and impact of secondary organic aerosol: current and emerging issues, *Atmos. Chem.*  
2 *Phys.*, 9, 5155-5236, 2009.

3 Harley, P., Fridd-Stroud, V., Greenberg, J., Guenther, A., and Vasconcellos, P.: Emission of 2-methyl-3-  
4 buten-2-ol by pines: A potentially large natural source of reactive carbon to the atmosphere, *J.*  
5 *Geophys. Res.*, 103, 25479-25486, 1998.

6 Hens, K., Novelli, A., Martinez, M., Auld, J., Axinte, R., Bohn, B., Fischer, H., Keronen, P., Kubistin, D.,  
7 Nölscher, A. C., Oswald, R., Paasonen, P., Petäjä, T., Regelin, E., Sander, R., Sinha, V., Sipilä, M.,  
8 Taraborrelli, D., Tatum Ernest, C., Williams, J., Lelieveld, J., and Harder, H.: Observation and  
9 modelling of HO<sub>x</sub> radicals in a boreal forest, *Atmos. Chem. Phys. Discuss.*, 13, 28561-28629,  
10 10.5194/acpd-13-28561-2013, 2013.

11 Hewitt, C. N., Kok, G. L., and Fall, R.: Hydroperoxides in plants exposed to ozone mediate air pollution  
12 damage to alkene emitters, *Nature*, 344, 56-57, 1990.

13 Hofzumahaus, A., Rohrer, F., Lu, K., Bohn, B., Brauers, T., Chang, C.-C., Fuchs, H., Holland, F., Kita, K.,  
14 Kondo, Y., Li, X., Lou, S., Shao, M., Zeng, L., Wahner, A., and Zhang, Y.: Amplified Trace Gas Removal  
15 in the Troposphere, *Science*, 324, 1702-1704, 10.1126/science.1164566, 2009.

16 Hogg, A., Uddling, J., Ellsworth, D., Carroll, M. A., Pressley, S., Lamb, B., and Vogel, C.: Stomatal and non-  
17 stomatal fluxes of ozone to a northern mixed hardwood forest, *Tellus Series B-Chemical And*  
18 *Physical Meteorology*, 59, 514-525, 2007.

19 Holzinger, R., Lee, A., Paw U, K. T., and Goldstein, A. H.: Observations of oxidation products above a  
20 forest imply biogenic emissions of very reactive compounds, *Atmos. Chem. Phys.*, 5, 67-75, 2005.

21 Hornbrook, R. S., Crawford, J. H., Edwards, G. D., Goyea, O., Maudlin III, R. L., Olson, J. S., and Cantrell, C.  
22 A.: Measurements of tropospheric HO<sub>2</sub> and RO<sub>2</sub> by oxygen dilution modulation and chemical  
23 ionization mass spectrometry, *Atmos. Meas. Tech.*, 4, 735-756, 10.5194/amt-4-735-2011, 2011.

24 Jenkin, M. E., Saunders, S. M., and Pilling, M. J.: The tropospheric degradation of volatile organic  
25 compounds: A protocol for mechanism development, *Atmos. Environ.*, 31, 81-104, 1997.

26 Karl, T., Hansel, A., Cappellin, L., Kaser, L., Herdinger-Blatt, I., and Jud, W.: Selective measurements of  
27 isoprene and 2-methyl-3-buten-2-ol base on NO<sup>+</sup> ionization mass spectrometry, *Atmos. Chem.*  
28 *Phys.*, 12, 11877-11884, 10.5194/acp-12-11877-2012, 2012.

29 Kaser, L., Karl, T., Guenther, A., Graus, M., Schnitzhofer, R., Turnipseed, A., Fischer, L., Harley, P.,  
30 Madronich, M., Gochis, D., Keutsch, F. N., and Hansel, A.: Undisturbed and disturbed above canopy  
31 ponderosa pine emissions: PTR-TOF-MS measurements and MEGAN 2.1 model results, *Atmospheric*  
32 *Chemistry and Physics Discussions*, 13, 15333-15375, 10.5194/acpd-13-15333-2013, 2013a.

33 Kaser, L., Karl, T., Schnitzhofer, R., Graus, M., Herdinger-Blatt, I. S., DiGangi, J. P., Sive, B., Turnipseed, A.,  
34 Hornbrook, R. S., Zheng, W., Flocke, F. M., Guenther, A., Keutsch, F. N., Apel, E., and Hansel, A.:  
35 Comparison of different real time VOC measurement techniques in a ponderosa pine forest, *Atmos.*  
36 *Chem. Phys.*, 13, 2893-2906, 10.5194/acp-13-2893-2013, 2013b.

37 Kim, S., Wolfe, G. M., Mauldin, R. L., Cantrell, C., Guenther, A., Karl, T., Turnipseed, A., Greenberg, J.,  
38 Hall, S. R., Ullmann, K., Apel, E., Hornbrook, R. S., Kajii, Y., Nakashima, Y., Keutsch, F. N., DiGangi, J.  
39 P., Henry, S. B., Kaser, L., Schnitzhofer, R., Graus, M., Hansel, A., Zheng, W., and Flocke, F. F.:  
40 Evaluation of HO<sub>x</sub> sources and cycling using measurement-constrained model calculations in a 2-  
41 methyl-3-butene-2-ol (MBO) and monoterpene (MT) dominated ecosystem, *Atmos. Chem. Phys.*, 13,  
42 2031-2044, 10.5194/acp-13-2031-2013, 2013.

- 1 Kirchner, F., Mayer-Figge, A., Zabel, F., and Becker, K. H.: Thermal Stability of Peroxynitrates, *Int. J.*  
2 *Chem. Kinet.*, 31, 127-144, 1999.
- 3 Kurpius, M. R., and Goldstein, A. H.: Gas-phase chemistry dominates O<sub>3</sub> loss to a forest, implying a  
4 source of aerosols and hydroxyl radicals to the atmosphere, *Geophys. Res. Lett.*, 30, 1371-1374,  
5 10.1029/2002GL016785, 2003.
- 6 LaFranchi, B. W., Wolfe, G. M., Thornton, J. A., Harrold, S. A., Browne, E. C., Min, K. E., Wooldridge, P. J.,  
7 Bilman, J. B., Kuster, W. C., Goldan, P. D., de Gouw, J. A., McKay, M., Goldstein, A. H., Ren, X., Mao,  
8 J., and Cohen, R. C.: Closing the peroxy acetyl nitrate budget: observations of acyl peroxy nitrates  
9 (PAN, PPN, and MPAN) during BEARPEX 2007, *Atmos. Chem. Phys.*, 9, 7623-7641, 2009.
- 10 Lelieveld, J., Butler, T. M., Crowley, J. N., Dillon, T. J., Fischer, H., Ganzeveld, L., Harder, H., Lawrence, M.  
11 G., Martinez, M., Taraborrelli, D., and Williams, J.: Atmospheric oxidation capacity sustained by a  
12 tropical forest, *Nature*, 452, 737-740, 10.1038/nature06870, 2008.
- 13 Liu, Y. J., Herdinger-Blatt, I., McKinney, K. A., and Martin, S. T.: Production of methyl vinyl ketone and  
14 methacrolein via the hydroperoxyl pathway of isoprene oxidation, *Atmospheric Chemistry and*  
15 *Physics*, 13, 5715-5730, 10.5194/acp-13-5715-2013, 2013.
- 16 Lou, S., Holland, F., Rohrer, F., Lu, K., Bohn, B., Brauers, T., Chang, C. C., Fuchs, H., Haseler, R., Kita, K.,  
17 Kondo, Y., Li, X., Shao, M., Zeng, L., Wahner, A., Zhang, Y., Wang, W., and Hofzumahaus, A.:  
18 Atmospheric OH reactivities in the Pearl River Delta - China in summer 2006: measurement and  
19 model results, *Atmos. Chem. Phys.*, 10, 11243-11260, 2010.
- 20 Makar, P. A., Fuentes, J. D., Wang, D., Staebler, R. M., and Wiebe, H. A.: Chemical processing of biogenic  
21 hydrocarbons within and above a temperate deciduous forest, *J. Geophys. Res.*, 104, 3581-3603,  
22 1999.
- 23 Mao, J., Ren, X., Brune, W. H., Van Duin, D. M., Cohen, R. C., Park, J. H., Goldstein, A. H., Paulot, F.,  
24 Beaver, M. R., Crouse, J. D., Wennberg, P. O., DiGangi, J. P., Henry, S. B., Keutsch, F. N., Park, C.,  
25 Schade, G. W., Wolfe, G. M., and Thornton, J. A.: Insights into hydroxyl measurements and  
26 atmospheric oxidation in a California forest, *Atmospheric Chemistry and Physics*, 12, 8009-8020,  
27 2012.
- 28 Mao, J., Paulot, F., Jacob, D. J., Cohen, R. c., Crouse, J. D., Wennberg, P. O., Keller, C. A., Hudman, R. C.,  
29 Barkley, M. P., and Horowitz, L. W.: Ozone and organic nitrates over the eastern United States:  
30 Sensitivity to isoprene chemistry, *Journal of Geophysical Research*, 118, 11256-11268,  
31 10.1002/jgrd.50817, 2013.
- 32 Mauldin, R., Berndt, T., Sipila, M., Paasonen, P., Petaja, T., Kim, S., Kurten, T., Stratmann, F., Kerminen,  
33 V., and Kulmala, M.: A new atmospherically relevant oxidant of sulphur dioxide, *Nature*, 488, 193-  
34 197, 10.1038/nature11278, 2012.
- 35 Mihele, C. M., and Hastie, D. R.: Radical chemistry at a forested continental site: Results from the  
36 PROPHET 1997 campaign, *J. Geophys. Res.*, 108, 4450-4460, 10.1029/2002JD002888, 2003.
- 37 Mogensen, D., Smolander, S., Sogachev, A., Zhou, L., Sinha, V., Guenther, A., Williams, J., Nieminen, T.,  
38 Kajos, M. K., Rinne, J., Kulmala, M., and Boy, M.: Modelling atmospheric OH-reactivity in a boreal  
39 forest ecosystem, *Atmospheric Chemistry And Physics*, 11, 9709-9719, 2011.
- 40 Moxim, W. J., Levy II, H., and Kasibhatla, P. S.: Simulated global tropospheric PAN: Its transport and  
41 impact on NO<sub>x</sub>, *J. Geophys. Res.*, 101, 12621-12638, 1996.

1 Nakashima, Y., Kato, S., Greenberg, J., Harley, P., Karl, T., Turnipseed, A., Apel, E., Guenther, A., Smith, J.,  
2 and Kajii, Y.: Total OH reactivity measurements in ambient air in a southern Rocky mountain  
3 ponderosa pine forest during BEACHON-SRM08 summer campaign, *Atmospheric Environment*, 85,  
4 1-8, <http://dx.doi.org/10.1016/j.atmosenv.2013.11.042>, 2014.

5 Nölscher, A. C., Williams, J., Sinha, V., Custer, T., Song, W., Johnson, A. M., Axinte, R., Bozem, H., Fischer,  
6 H., Pouvesle, N., Phillips, G., Crowley, J. N., Rantala, P., Rinne, J., Kulmala, M., Gonzales, D., Valverde-  
7 Canossa, J., Vogel, A., Hoffmann, T., Ouwersloot, H. G., Vila-Guerau de Arellano, J., and Lelieveld, J.:  
8 Summertime total OH reactivity measurements from boreal forest during HUMPPA-COPEC 2010,  
9 *Atmos. Chem. Phys.*, 12, 8257-8270, 10.5194/acp-12-8257-2012, 2012.

10 Ortega, J., Turnipseed, A., Guenther, A. B., Karl, T. G., Day, D. A., Gochis, D., Huffman, J. A., Prenni, A. J.,  
11 Levin, E. J. T., Kreidenweis, S. M., DeMott, P. J., Tobo, Y., Patton, E. G., Hodzic, A., Cui, Y., Harley, P.  
12 C., Hornbrook, R. H., Apel, E. C., Monson, R. K., Eller, A. S. D., Greenberg, J. P., Barth, M.,  
13 Campuzano-Jost, P., Palm, B. B., Jimenez, J. L., Aiken, A. C., Dubey, M. K., Geron, C., Offenberg, J.,  
14 Ryan, M. G., Fornwalt, P. J., Pryor, S. C., Keutsch, F. N., DiGangi, J. P., Chan, A. W. H., Goldstein, A. H.,  
15 Wolfe, G. M., Kim, S., Kaser, L., Schnitzhofer, R., Hansel, A., Cantrell, C. A., Mauldin lii, R. L., and  
16 Smith, J. N.: Overview of the Manitou Experimental Forest Observatory: site description and  
17 selected science results from 2008&ndash;2013, *Atmos. Chem. Phys. Discuss.*, 14, 1647-1709,  
18 10.5194/acpd-14-1647-2014, 2014.

19 Paulot, F., Henze, D. K., and Wennberg, P. O.: Impact of the isoprene photochemical cascade on tropical  
20 ozone, *Atmos. Chem. Phys.*, 12, 1307-1325, 2012.

21 Peeters, J., Nguyen, T. L., and Vereecken, L.: HOx radical regeneration in the oxidation of isoprene, *Phys.*  
22 *Chem. Chem. Phys.*, 11, 5935-5939, 2009.

23 Peeters, J., and Müller, J. F.: HOx radical regeneration in isoprene oxidation via peroxy radical  
24 isomerisations. II: experimental evidence and global impact, *Phys. Chem. Chem. Phys.*, 12, 14227-  
25 14235, 2010.

26 Qi, B., Takami, A., and Hatakeyama, S.: Peroxy radical concentrations measured at a forest canopy in  
27 Nikko, Japan, in summer 2002, *J. Atmos. Chem.*, 52, 63-79, 2005.

28 Ren, X. R., Olson, J. R., Crawford, J. H., Brune, W. H., Mao, J. Q., Long, R. B., Chen, Z., Chen, G., Avery, M.  
29 A., Sachse, G. W., Barrick, J. D., Diskin, G. S., Huey, L. G., Fried, A., Cohen, R. C., Heikes, B.,  
30 Wennberg, P. O., Singh, H. B., Blake, D. R., and Shetter, R. E.: HOx chemistry during INTEX-A 2004:  
31 Observation, model calculation, and comparison with previous studies, *J. Geophys. Res. Atmos.*, 113,  
32 D05310, 10.1029/2003JD003551 2008.

33 Saunders, S. M., Jenkin, M. E., Derwent, R. G., and Pilling, M. J.: Protocol for the development of the  
34 Master Chemical Mechanism, MCM v3 (Part A): tropospheric degradation of non-aromatic volatile  
35 organic compounds, *Atmos. Chem. Phys.*, 3, 161-180, 2003.

36 Seok, B., Helmig, D., Ganzeveld, L., Williams, M. W., and Vogel, C. S.: Dynamics of nitrogen oxides and  
37 ozone above and within a mixed hardwood forest in northern Michigan, *Atmospheric Chemistry and*  
38 *Physics*, 13, 7301-7320, 10.5194/acp-13-7301-2013, 2013.

39 Shu, Y., and Atkinson, R.: Rate Constants for the Gas-Phase Reactions of O<sub>3</sub> with a Series of Terpenes and  
40 OH Radical Formation from the O<sub>3</sub> Reactions with Sesquiterpenes at 296 ± 2 K, *Int. J. Chem. Kinet.*,  
41 26, 1193 - 1205, 1994.

1 Sinha, V., Williams, J., Lelieveld, J., Ruuskanen, T. M., Kajos, M. K., Patokoski, J., Hellen, H., Hakola, H.,  
2 Mogensen, D., Boy, M., Rinne, J., and Kulmala, M.: OH Reactivity Measurements within a Boreal  
3 Forest: Evidence for Unknown Reactive Emissions, *Environ. Sci. Technol.*, 44, 6614-6620, 2010.

4 Sommariva, R., Bates, T. S., Bon, D., Brookes, D. M., de Gouw, J. A., Gilman, J. B., Herndon, S. C., Kuster,  
5 W. C., Lerner, B. M., Monks, P. S., Osthoff, H. D., Parker, A. E., Roberts, J. M., Tucker, S. C., Warneke,  
6 C., Williams, E. J., Zahniser, M. S., and Brown, S. S.: Modelled and measured concentrations of  
7 peroxy radicals and nitrate radical in the U.S. Gulf Coast region during TexAQS 2006, *J. Atmos.*  
8 *Chem.*, 68, 331-362, 10.1007/s10874-012-9224-7, 2011.

9 Sparks, J. P., Walker, J., Turnipseed, A., and Guenther, A.: Dry nitrogen deposition estimates over a  
10 forest experiencing free air CO<sub>2</sub> enrichment, *Global Change Biology*, 14, 768-781, 2008.

11 Stavrou, T., Peeters, J., and Müller, J.-F.: Improved global modelling of HO<sub>x</sub> recycling in isoprene  
12 oxidation: evaluation against the GABRIEL and INTEX-A aircraft campaign measurements, *Atmos.*  
13 *Chem. Phys.*, 10, 9863-9878, 10.5194/acp-10-9863-2010, 2010.

14 Stone, D., Whalley, L. K., and Heard, D. E.: Tropospheric OH and HO<sub>2</sub> radicals: field measurements and  
15 model comparisons, *Chem. Soc. Rev.*, 41, 6348-6404, 10.1039/C2CS35140D, 2012.

16 Tan, D., Faloon, I., Simpas, J. B., Brune, W., Shepson, P. B., Couch, T. L., Sumner, A. L., Carroll, M. A.,  
17 Thornberry, T., Apel, E., Riemer, D., and Stockwell, W.: HO<sub>x</sub> budgets in a deciduous forest: Results  
18 from the PROPHET summer 1998 campaign, *J. Geophys. Res. Atmos.*, 106, 24407-24427, 2001.

19 Thornton, J. A., Wooldridge, P. J., Cohen, R. C., Martinez, M., Harder, H., Brune, W. H., Williams, E. J.,  
20 Roberts, J. M., Fehsenfeld, F. C., Hall, S. R., Shetter, R. E., Wert, B. P., and Fried, A.: Ozone production  
21 rates as a function of NO<sub>x</sub> abundances and HO<sub>x</sub> production rates in the Nashville urban plume, *J.*  
22 *Geophys. Res.*, 107, 4146-4163, 10.1029/2001JD000932, 2002.

23 Whalley, L. K., Edwards, P. M., Furneaux, K. L., Goddard, A., Ingham, T., Evans, M. J., Stone, D., Hopkins,  
24 J. R., Jones, C. E., Karunaharan, A., Lee, J. D., Lewis, A. C., Monks, P. S., Moller, S. J., and Heard, D. E.:  
25 Quantifying the magnitude of a missing hydroxyl radical source in a tropical rainforest, *Atmos.*  
26 *Chem. Phys.*, 11, 7223-7233, 2011.

27 Whalley, L. K., Blitz, M. A., Desservettaz, M., Seakins, P. W., and Heard, D. E.: Reporting the sensitivity of  
28 Laser Induced Fluorescence instruments used for HO<sub>2</sub> detection to an interference from RO<sub>2</sub>  
29 radicals and introducing a novel approach that enables HO<sub>2</sub> and certain RO<sub>2</sub> types to be selectively  
30 measured, *Atmospheric Measurement Techniques Discussions*, 6, 6249-6292, 10.5194/amtd-6-  
31 6249-2013, 2013a.

32 Whalley, L. K., Blitz, M. A., Desservettaz, M., Seakins, P. W., and Heard, D. E.: Reporting the sensitivity of  
33 laser-induced fluorescence instruments used for HO<sub>2</sub> detection to an interference from RO<sub>2</sub> radicals  
34 and introducing a novel approach that enables HO<sub>2</sub> and certain RO<sub>2</sub> types to be selectively  
35 measured, *Atmospheric Measurement Techniques*, 6, 3425-3440, 10.5194/amt-6-3425-2013, 2013b.

36 Wolfe, G. M., and Thornton, J. A.: The Chemistry of Atmosphere-Forest Exchange (CAFE) Model - Part 1:  
37 Model Description and Characterization, *Atmos. Chem. Phys.*, 11, 77-101, 2011.

38 Wolfe, G. M., Thornton, J. A., Bouvier-Brown, N. C., Goldstein, A. H., Park, J.-H., McKay, M., Matross, D.  
39 M., Mao, J., Brune, W. H., LaFranchi, B. W., Browne, E. C., Min, K.-E., Wooldridge, P. J., Cohen, R. C.,  
40 Crouse, J. D., Faloon, I. C., Gilman, J. B., Kuster, W. C., de Gouw, J. A., Huisman, A., and Keutsch, F.  
41 N.: The Chemistry of Atmosphere-Forest Exchange (CAFE) Model - Part 2: Application to BEARPEX-  
42 2007 observations, *Atmos. Chem. Phys.*, 11, 1269-1294, 2011a.

1 Wolfe, G. M., Thornton, J. A., McKay, M., and Goldstein, A. H.: Forest-atmosphere exchange of ozone:  
2 sensitivity to very reactive biogenic VOC emissions and implications for in-canopy photochemistry,  
3 Atmospheric Chemistry and Physics, 11, 7875-7891, 2011b.

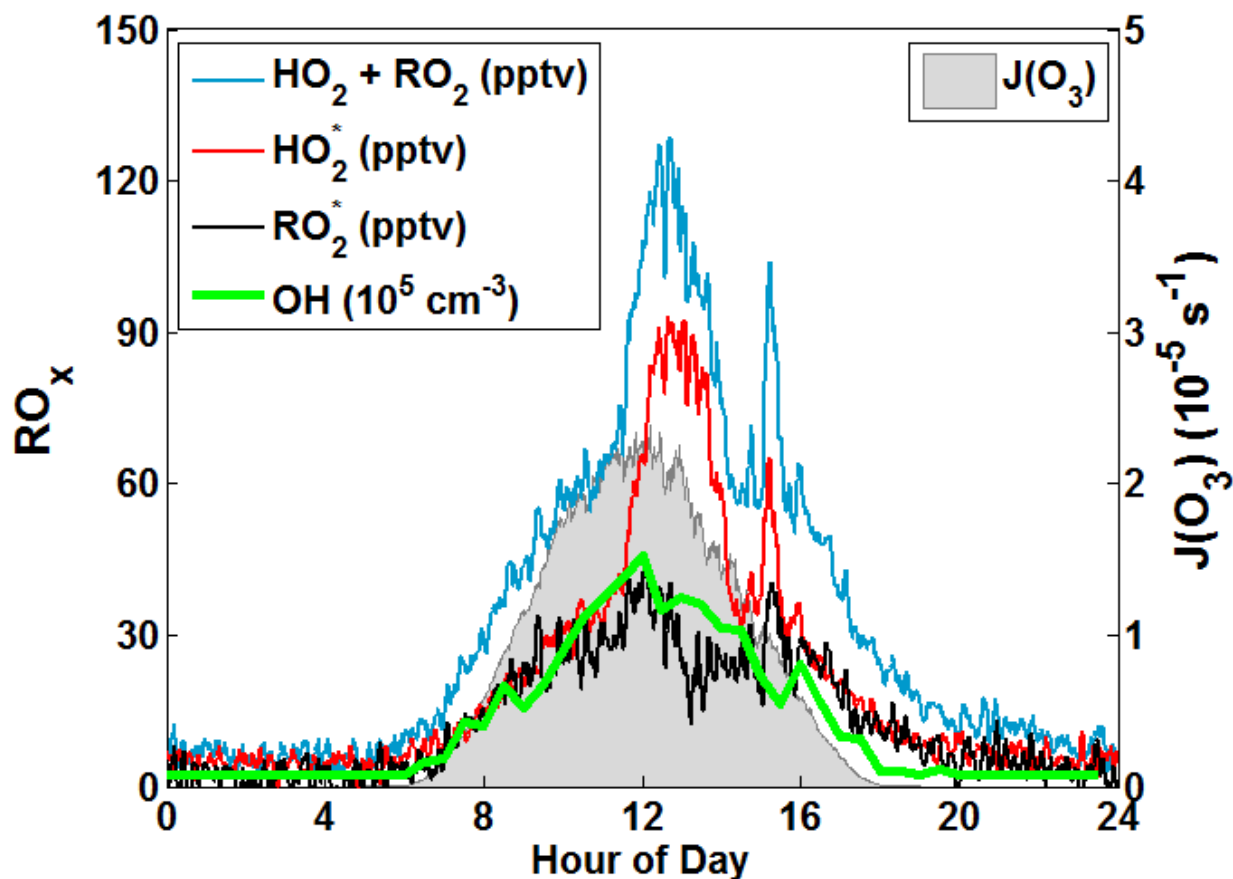
4 Wolfe, G. M., Crouse, J. D., Parrish, J. D., St. Clair, J. M., Beaver, M. R., Paulot, F., Yoon, T. P., Wennberg,  
5 P. O., and Keutsch, F. N.: Photolysis, OH reactivity and ozone reactivity of a proxy for isoprene-  
6 derived hydroperoxyenals (HPALDs), Phys. Chem. Chem. Phys., 14, 7276-7286,  
7 10.1039/C2CP40388A, 2012.

8 Wooldridge, P. J., Perring, A. E., Bertram, T. H., Flocke, F. M., Roberts, J. M., Singh, H. B., Huey, L. G.,  
9 Thornton, J. A., Wolfe, G. M., Murphy, J. G., Fry, J. L., Rollins, A. W., LaFranchi, B. W., and Cohen, R.  
10 C.: Total peroxy nitrates ( $\Sigma$ PNs) in the atmosphere: the thermal dissociation-laser induced  
11 fluorescence (TD-LIF) technique and comparisons to speciated PAN measurements, Atmos. Meas.  
12 Tech., 3, 593-607, 2010.

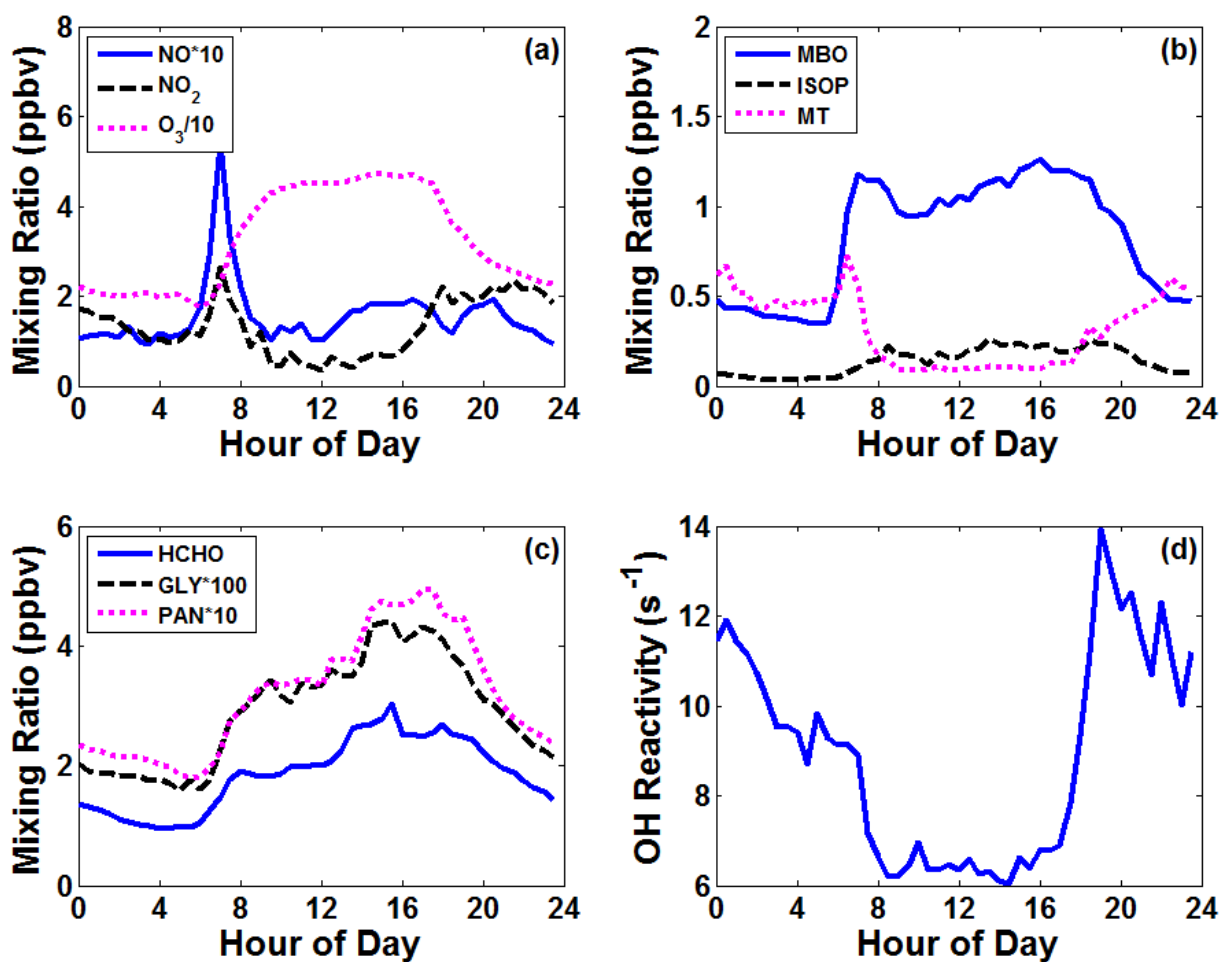
13 Xie, Y., Paulot, F., Carter, W. P. L., Nolte, C. G., Luecken, D. J., Hutzell, W. T., Wennberg, P. O., Cohen, R.  
14 C., and Pinder, R. W.: Understanding the impact of recent advances in isoprene photooxidation on  
15 simulations of regional air quality, Atmospheric Chemistry and Physics, 13, 8439-8455, 10.5194/acp-  
16 13-8439-2013, 2013.

17  
18  
19



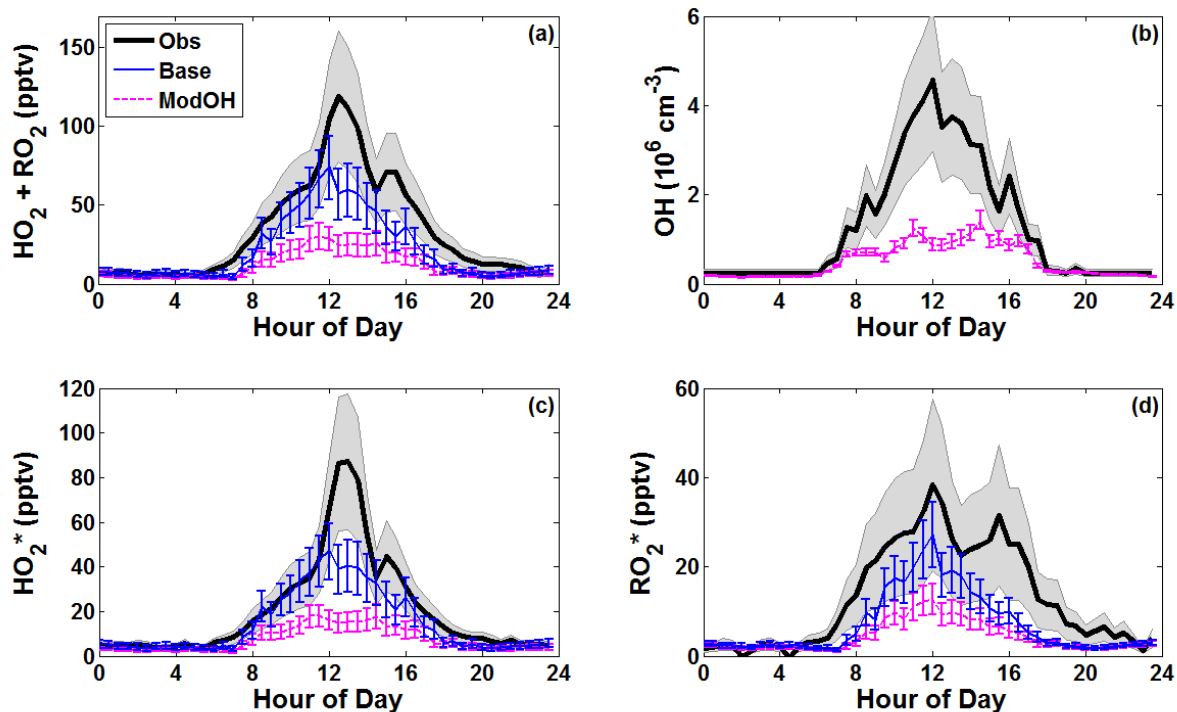


1  
 2  
 3  
 4 Figure 1. Average diel cycles of total peroxy radicals (blue), HO<sub>2</sub><sup>\*</sup> (red), RO<sub>2</sub><sup>\*</sup> (black), OH  
 5 (green) and ozone photolysis frequency (filled gray area). Peroxy radicals and J(O<sub>3</sub>) are shown as  
 6 1-minute means, while OH is displayed as a 30-minute mean. J(O<sub>3</sub>) is calculated by scaling  
 7 measured J(NO<sub>2</sub>) with the ratio of J(O<sub>3</sub>)/J(NO<sub>2</sub>) calculated from the MCM parameterization for  
 8 clear-sky conditions. Nighttime OH values were typically below the instrument detection limit (5  
 9 x 10<sup>5</sup> cm<sup>-3</sup>) and are thus set to half of this value.  
 10



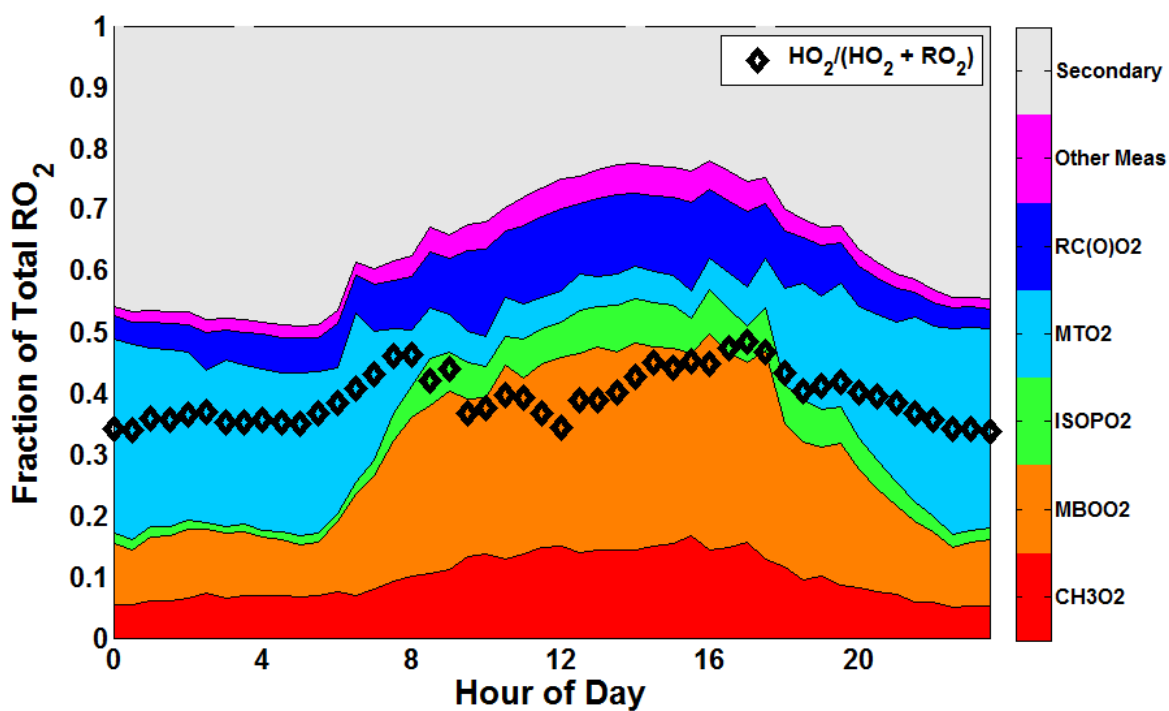
1  
2  
3  
4  
5  
6  
7

Figure 2. Average diel observations of (a) NO, NO<sub>2</sub> and ozone, (b) MBO, isoprene and total monoterpenes, (c) formaldehyde, glyoxal and PAN, and (d) OH reactivity. All data are 30-minute means. Note that some species have been scaled to fit on a single axis, as denoted in the plot legends.



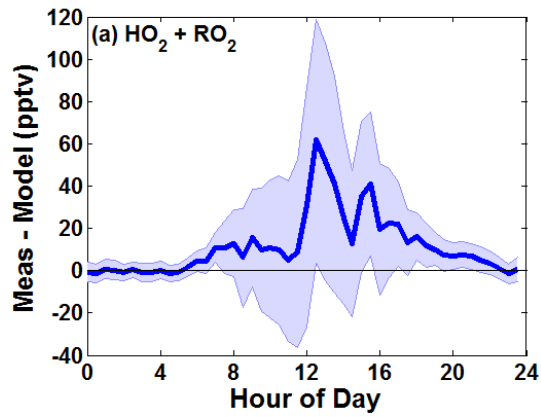
1  
2  
3  
4  
5  
6  
7  
8  
9  
10

Figure 3. Comparison of  $\text{RO}_x$  observations with 0-D model results. Solid black lines with shaded gray areas represent observations and their associated uncertainties. Model scenarios include the base (solid blue line) and ModOH (dashed magenta line) simulations; in the latter case, OH concentrations are not constrained to observations. For comparison with  $\text{HO}_2^*$  and  $\text{RO}_2^*$  in (c) and (d), the total modeled  $\text{RO}_2$  is sub-divided into two groups as described in the text. Calculation of model uncertainties is described in the SI.

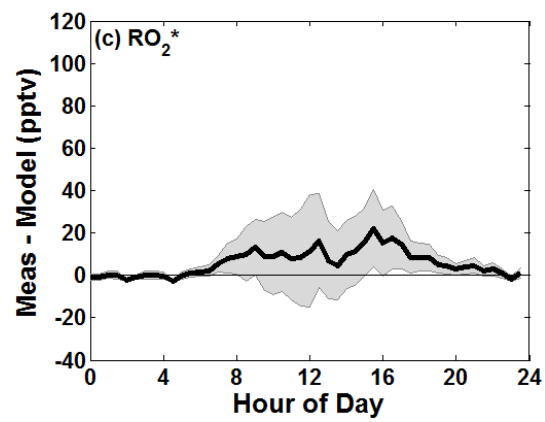
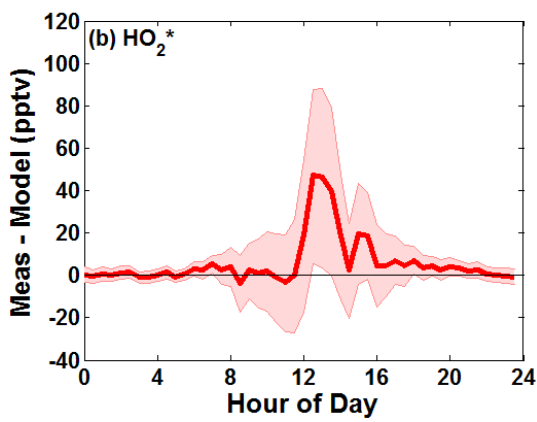


1  
2  
3  
4  
5  
6  
7  
8  
9

Figure 4. Modeled distribution of organic peroxy radicals from the base simulation. Groups include methyl peroxy radical (red), first-generation peroxy radicals of MBO (yellow), isoprene (green) and monoterpenes (cyan), total acyl peroxy radicals (blue), first-generation radicals from oxidation of other measured VOC (magenta), and “secondary” radicals resulting from oxidation of model-predicted, unmeasured VOC (gray). The ratio of HO<sub>2</sub> to total peroxy radicals is also shown (black diamonds).



1

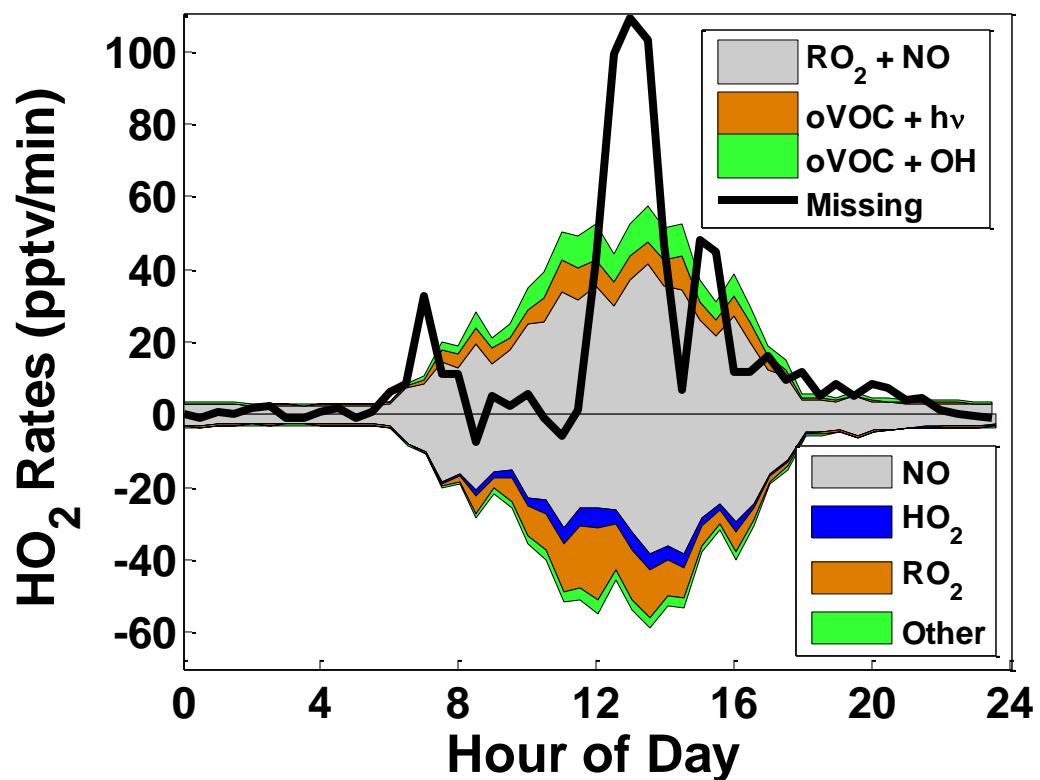


2

3

4 Figure 5. Difference between observed and modeled peroxy radical mixing ratios: (a) total  
 5 peroxy radicals, (b)  $\text{HO}_2^*$  and (c)  $\text{RO}_2^*$ . Model values are taken from the base simulation.  
 6 Shaded areas represent the combined uncertainty from observed and modeled mixing ratios.

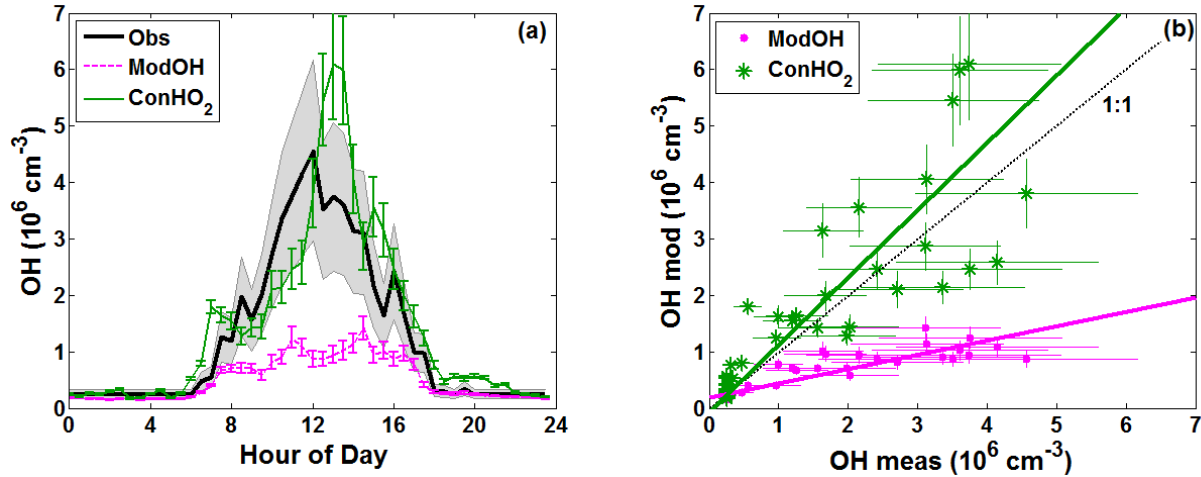
7



1

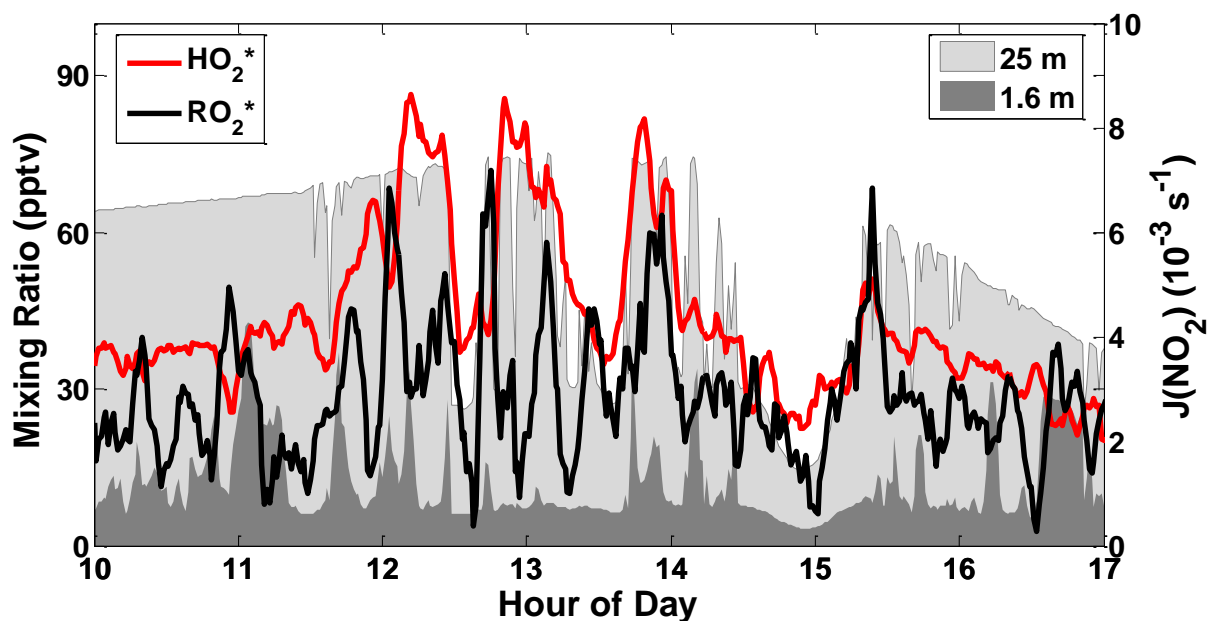
2

3 Figure 6. Rates of HO<sub>2</sub> production and loss calculated from the base model scenario. Rates are  
 4 grouped according to the type of reaction. Production includes reaction of RO<sub>2</sub> with NO (gray),  
 5 VOC photolysis (orange) and OH oxidation of VOC (green). Losses include reactions with NO  
 6 (gray), HO<sub>2</sub> (blue), RO<sub>2</sub> (orange) and OH and ozone (green). The thick black line denotes the  
 7 proposed missing HO<sub>2</sub> source, calculated as described in the text.



1  
2  
3  
4  
5  
6  
7  
8  
9  
10  
11

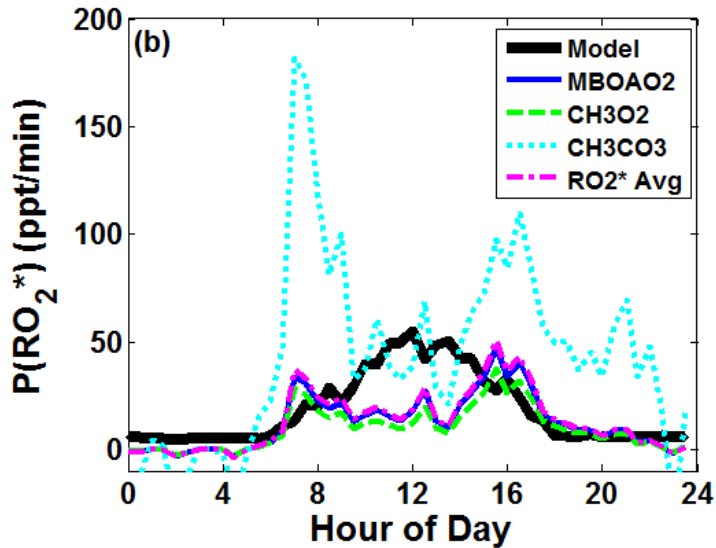
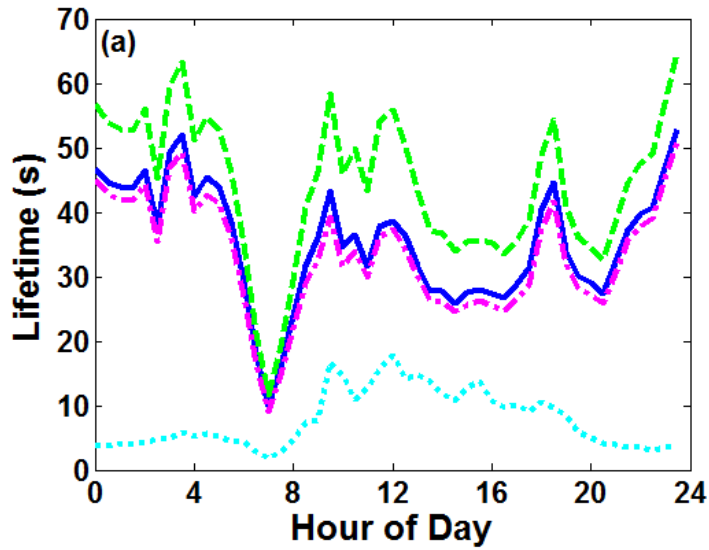
Figure 7. Comparison of measured and modeled OH concentrations. (a) Diurnal profiles. Observations and their uncertainties are shown as a black line with grey shading. The ModOH results (magenta) are the same as those shown in Fig. 3. In the HO<sub>2</sub>-constrained case (green), HO<sub>2</sub> is constrained to “missing” HO<sub>2</sub>\* as described in Sec. 5.1. The same uncertainties are assumed for both model scenarios. (b) Scatter plot of the same results for ModOH (magenta dots) and HO<sub>2</sub>-constrained (green asterisks) scenarios. Thin lines define uncertainties in modeled and measured values. Thick lines represent uncertainty-weighted major axis regression fits (ModOH:  $y = 0.24x + 0.18$ ,  $r^2 = 0.81$ ; ConHO<sub>2</sub>:  $y = 1.19x - 0.05$ ,  $r^2 = 0.75$ ).



1  
2  
3  
4  
5  
6  
7

Figure 8. Example of fast mid-day variations of solar radiation and peroxy radicals for day 234 (22 Aug). HO<sub>2</sub>\* (red) and RO<sub>2</sub>\* (black) are plotted on the left axis, while NO<sub>2</sub> photolysis frequencies are plotted on the right axis for both above-canopy (light gray) and below-canopy (dark gray) measurements. All data are 1-minute averages.





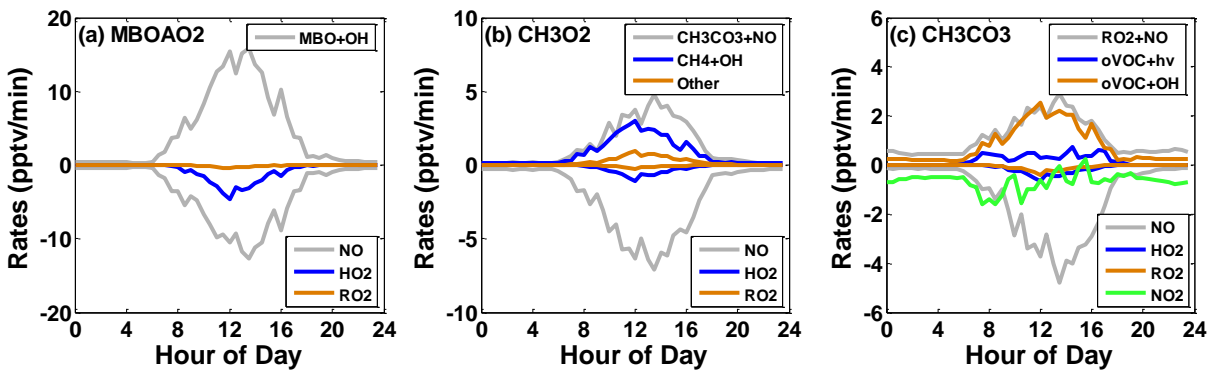
1

2

3

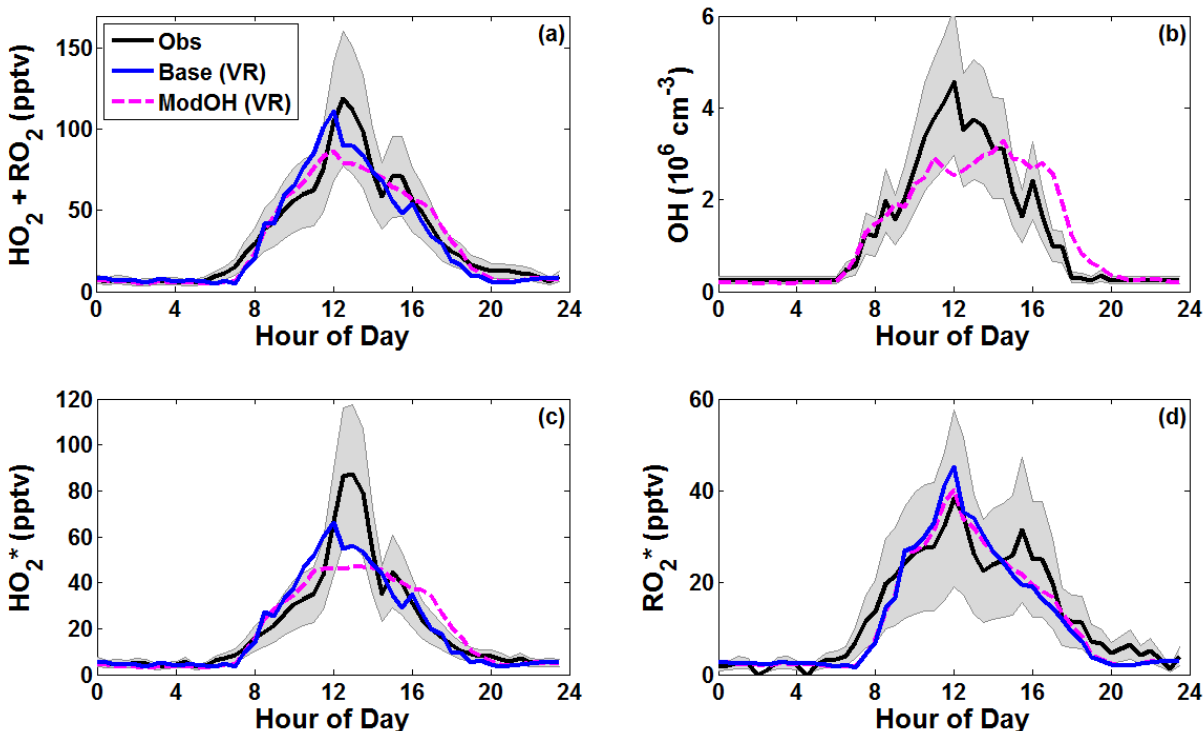
4 Figure 9. (a) Modeled chemical lifetimes for several representative species: MBOAO2 (solid  
 5 blue line), methyl peroxy radical (dashed green line) and acetyl peroxy radical (dashed cyan  
 6 line). The concentration-weighted average  $RO_2^*$  lifetime is also shown (dash-dotted magenta  
 7 line). (b) Missing  $RO_2^*$  production rates calculated as described in the text. Also shown is the  
 8 total production rate for all modeled  $RO_2^*$  (thick black line). Model results are taken from the  
 9 base simulation.

10



1  
2  
3  
4  
5  
6  
7

Figure 10. Modeled chemical tendencies for three representative organic peroxy radicals: (a) MBOAO<sub>2</sub>, (b) methyl peroxy radical and (c) acetyl peroxy radical. In (c), the loss rate attributed to NO<sub>2</sub> (green line) represents the net effect of PAN production and decomposition. Model results are taken from the base simulation.



1  
2  
3  
4  
5  
6  
7  
8  
9  
10

Figure 11. Comparison of  $\text{RO}_x$  observations with 0-D model results using the very reactive VOC mechanism. Solid black lines with shaded gray areas represent observations and their associated uncertainties. Model simulations include the base (solid blue line) and ModOH (dashed magenta line) scenarios augmented with very reactive VOC chemistry; in the latter case, OH concentrations are not constrained to observations. For comparison with  $\text{HO}_2^*$  and  $\text{RO}_2^*$  in (c) and (d), the total modeled  $\text{RO}_2$  is sub-divided into two groups as described in the text. Model uncertainties are excluded for clarity.